國立臺灣大學大氣科學系

碩士論文

Department of Atmospheric Sciences

College of Science

National Taiwan University

Master Thesis

重力波動對層積雲系統垂直結構及雲量之影響

Impact of Gravity Waves on Marine Stratocumulus
Variability: Vertical Structures and Cloud Coverage

林佑宇

Yu-Yu Lin

指導教授：郭鴻基 博士、吳健銘 博士

Advisor: Hung-Chi Kuo, Ph.D.、Chien-Ming Wu, Ph.D.

中華民國 104 年 7 月

July 2015

致謝

本論文的完成，幸蒙郭鴻基老師和吳健銘老師的指導與教誨，對於研究的方向、觀念的啟迪、邏輯架構的訓練、求學的態度逐一斧正與細細關懷，於此獻上最深的敬意與謝意。論文口試期間，承蒙文化大學蘇世顥教授、台灣大學羅敏輝教授及黃彥婷教授細心的指導批評，多謝口試委員們的費心審閱，並惠賜諸多建議，使本論文增色許多。

兩年的日子點滴在心頭，實驗室裡的生活點滴，感謝學長姐、同學、學弟妹的共同砥礪。在口試期間承蒙各位的指導批評，在最後修正了許多邏輯架構的問題及圖片的潤飾，在這期間從各位的身上學到的實在是太多了，心中除了感謝還是感謝，謝謝你們。

在生活上，感謝家人兩年來的關懷與包容，奶奶儘管身體不適還是總是先關心我的學業，論文的完成，各位是我最大的動力，謝謝。

此外，特別感謝 B98 的各位好同學們，一路跌跌撞撞走了 6 年，總有離別的一天，今後真的要離開台大了，細數過往的回憶，在各位身上學到了好多，感謝冠廷、文瑛、晉安、俊彥在研究上模式問題的幫助和研究題目上的討論。各位的陪伴讓兩年的研究生活變得絢麗多彩，祝各位未來研究步步高升，兵役期間一切平安順遂，鵬任、徐辛未來一年的研究順利，也恭喜即將退伍的家名，邁向人生的下一里程碑。

最後，謹以此文獻給我摯愛的雙親。

佑宇 謹誌於

台灣大學大氣科學研究所

中華民國一零四年八月

摘要

本研究主要探討邊界層層積雲在中尺度重力波動下的結構變化，利用三維雲解析模式(Vector Vorticity Model)做為模擬工具，透過北美加州外海 DYCOMS-II 機載觀測資料和南美智利外海 VOCALS RV brown 觀測船之探空當作模式之初始條件，研究短周期(3 小時)和半日周期的中尺度重力波動對邊界層層積雲結構之影響。

實驗結果發現對於短周期的波動而言，從量化的分層診斷參數 BIR(buoyancy Integral Ratio) 和總水混合比差異(Total Water Mixing Ratio Difference)顯示對邊界層層積雲的結構沒有重大的影響，在實驗結束之後邊界層仍然處於均勻混合的狀態，邊界層頂下的層積雲仍維持一樣的覆蓋率；相反地，在半日周期之波動結果顯示 DYCOMS-II 和 VOCALS 兩組實驗，邊界層皆發生了顯著的分層現象(decoupling)，原均勻混合的邊界層分離為上層層積雲覆蓋之混合殘餘層和下層受海表能量和水氣通量影響之混合層。進一步診斷發現 VOCALS 在分層的情況下其上層的層積雲無法穩定維持，受重力波動影響幾近完全消散；DYCOMS-II 則仍穩定的維持其層積雲雲層，其最主要差異為分層後下層的積雲活動強度之差異，對於 VOCALS 剖面其海表的水氣和能量通量較弱，因此上升氣流強度較弱，又 VOCALS 剖面其邊界層的高度較高，下層海表的氣塊不易上升至舉升凝結高度之上形成積雲，而此積雲能短暫的與上層層積雲偶合，輸送水氣和能量至上層幫助維持上層的雲層。因此對於 VOCALS 剖面其下層的積雲活動強度較弱，使得上層層積雲無法穩定維持。

關鍵字: 邊界層;層積雲;邊界層分離;中尺度重力波動;表面通量。

Abstract

This study aims to understand the impacts of gravity waves on the cloud fraction and vertical structures of stratocumulus topped boundary layer (STBL) under two stratocumulus regimes. The impact of such gravity waves on STBL is investigated using a high-resolution vector vorticity equation based cloud resolving model (VVM) (Jung and Arakawa 2008; Wu and Arakawa 2011) by adding large-scale convergence that mimics observed mesoscale semidiurnal waves.
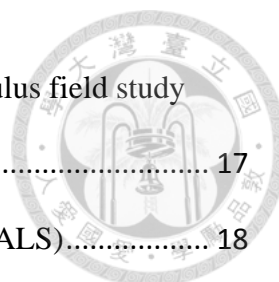
The results show that the wave induced vertical velocity causes STBL to become decoupled. During the ascending phase, the cloud is lifted and thickens. With larger cloud amount, Entrainment-Liquid Flux feedback (ELF) starts to adjust by enhancing cloud top entrainment and cloud base warming, which causes STBL to become decoupled. Furthermore, the results show that the vertical structure and cloud fraction at the end of simulation is largely determined by the sea surface fluxes. The experiment with weaker surface fluxes causes STBL to break up by limiting Surface-based Mixed Layer (SML) cumuliform clouds.

Keywords: stratocumulus; upsidence wave; decoupling; entrainment; surface flux; stratocumulus-topped boundary layer; STBL.

Contents

Figure Captions

Table Captions

1. Introduction

Marine stratocumulus clouds play an important role in the climate system. First of all, such low level clouds can largely reflect the incoming solar radiation compared to sea surface. Secondly, they form at low level so that the outgoing long wave radiation between stratocumulus covered or clear sky condition remain about the same. So the net radiative effect of stratocumulus on earth system is reducing the energy input into the earth system.

They are generally thin clouds, occupying upper planetary boundary layer, so called Stratocumulus-Topped Boundary Layer, hereafter STBL, and tends to form under stable lower-tropospheric conditions (over the subtropics, Hadley Cell subsidence region). The development and evolution of stratocumulus is tightly relative to turbulence activity below boundary layer and interaction between eddies and large scale flow, such physics cannot well resolved by climate models, these sub-grid process can only tackle by parameterization, thus there still remain some uncertainty in future climate prediction regarding to modeling the stratocumulus deck because they reduce the earth's albedo and thus decrease the energy input into the earth system.

In this chapter, we first review the conceptual model of the formation of stratocumu-

lus by Robert A. house shown in Fig.1. Then briefly examine the important physical process controlling the development of stratocumulus and vertical structures of Stratocumulus-Topped Boundary Layer. Lastly, introduce recent numerical research relative to our study on the stratocumulus about adjustment time scale.
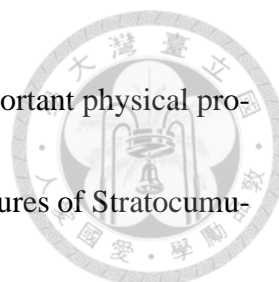
1.1 The formation of stratocumulus

The formation of stratocumulus upon boundary layer top can be realized as follows: firstly, the boundary layer is characterized by a population of thermo bubbles or buoyant plumes forming at sea surface due to surface heating by solar radiation or surface wind shear. Subsequently, the boundary layer becomes well-mixed as a result of upward energy fluxes. At the same time, the boundary layer top entrain upper atmospheric air so that the layer deepened. Secondly, as the depth of boundary layer increases, the height of updraft plumes above lifting condensation level forming small cloud patches. Lastly, the cloud gradually thickens to form a more continuous sheet of cloud at the top of boundary layer.

1.2 Physical process involved in stratocumulus

1.2.1 Cloud top radiative cooling and sea surface fluxes

Cloud top radiative cooling in most cases served as the leading term in turbulent kinetic energy budget. Such radiative cooling is confined at cloud top and below few

meters because most stratocumulus contain liquid water in sufficient abundance that they are largely opaque to longwave radiation. Besides the TKE issue, cloud top radiative cooling also drives the convections in STBL (Lilly 1968). Cloud top radiative divergence causes air parcel colder than environment. At the time parcel start sinking, thus driving the convection.

Sea surface is an important lower boundary for STBL. On the one hand, surface moisture flux provides ample moisture forming the stratocumulus cloud; on the other hand, surface heat flux, which is controlled by sea surface temperature, is one of the key factors regarding to stratocumulus transitions to trade wind cumulus issue.

Stratocumulus clouds often forming at the east side of the oceans seen in the Fig.1 (a), which characterized by the upwelling of cloud water onto the sea surface. The colder SST prevent stronger convection develop and thus the low level clouds are easier to form. Schubert et al. (1979a,b) and (Bretherton and Wyant 1997) investigate the influence of sea surface variation on stratocumulus, the result shows that SST has a profound effect on STBL. When SST rising along the equatorward return flow of Hadley cell, the cloud becomes thicker and more cumuliform cloud formed, and inversion height become higher, which in the last transit stratocumulus-topped boundary layer into shallow cumulus topped layer.

1.2.2   Entrainment and cloud top entrainment instability (CTEI)

Entrainment accounts for small-scale mixing process at the inversion top. It causes inversion height growth but at the same time, in most cases, entrains dry air into STBL, reducing the turbulent kinetic energy. Entrainment is also a major unresolved question in stratocumulus dynamics. Namely, how entrainment rate relate to STBL turbulent dynamics? This is still an open question. Regarding to observation issue, making an accurate measurements of the entrainment rate in STBL is difficult because the sharp inversion aloft the cloud coverage makes it hard to acquire accurate data. On the other hand, the small scale mixing process is also difficult to well resolve in numerical model, in most cases only through parameterization except LES models or DNS models.

As mentioned previously, entrainment brings upper dry air into STBL and will reduce TKE; however, in some cases it creates TKE. The process of mixing dry free-tropospheric air into the STBL can create negatively buoyant mixtures compare to the unmixed cloudy air. This occurs when dry aloft air mixed into cloudy air, causing cloud evaporation. In the last the evaporative cooling of cloud water generate colder air from environment and thus produce TKE. This so called buoyancy reversal had been thought leading to rapid runaway entrainment in a process known as cloud-top entrainment instability (CTEI) (Lilly 1968; Randall 1980). The instability criterion is:

$$\Delta\theta_e < \kappa \frac{L}{c_p} \Delta r \tag{1}$$

$$\kappa = \frac{(1+\gamma)c_p\theta_0/L}{1+(1+\delta)\gamma c_p\theta_0/L} = 0.23 \tag{2}$$

$$\gamma = \frac{L}{c_p}\frac{\partial q^*}{\partial\theta} \tag{3}$$

In which, L is the latent heat of vaporization、c_p is the specific heat capacity of dry air at constant pressure、q^* is the saturation water vapor mixing ratio.

Although this criterion is well formulated to capture the process of buoyancy reversal, observation shows that even such condition is satisfied, CTEI does not necessary cause cloud breaking. As shown by (Kuo and Schubert 1988 in Fig.3), which plot all observation data in $\Delta\theta_e - \frac{L}{c_p}\Delta r$ diagram. The results reveal that CTEI is not the only mechanism causing cloud breaking. There is other factors help maintain the clouds.

CTEI and cloud top radiative cooling both are the key features differentiate stratocumulus convection from cumulus convection. Randall(1980) called such convection as Conditional Instability of the First Kind Upside-down (CIFKU) because this type of convection is similar to Conditional Instability of the First Kind (CIFK) in cumulus convection, the main source of instability coming from buoyancy. Difference lies on how they release the instability: under CIFKU case, the cloud top cooling drives air parcel sinking

and generate kinetic energy; on the contrary, CIFK is caused by latent heat release by

condensation and thus drive the upward motion.

1.2.3   Large scale subsidence

As mentioned in *section 1.2.1*, stratocumulus clouds form at east side of the oceans.

Moreover, they usually form at the downward branch of Hadley cell seen in Fig.1 (a),

which characterize the weak subsidence in this region. Such weak subsidence helps main-

tain shallower PBL, inhibiting the development of deep convection. The colder SST and

weak subsidence both help restrain the deep convection and form the stratocumulus

clouds.

Since STBL is shallow, we can determine the subsidence rate in terms of large scale

divergence profile $D(z)$ through continuity equation. Divergence has an important influ-

ence on STBL structural and dynamical properties because it controls the inversion height,

which strongly relate to STBL structures. This relation is nonlinear since weak subsidence

results in deeper inversion height so that it decouples and can no longer support stratocu-

mulus; while strong subsidence can lower the inversion height even below the Lifting

Condensation Level (LCL), which leads to no clouds circumstance. For the typical sub-

tropical marine stratocumulus, the low level divergence is about $1 \times 10^{-6} \sim 4 \times 10^{-6} s^{-1}$.

1.3   Vertical structure of stratocumulus-topped boundary layer

As mentioned in *section 1.2*, STBL is controlled by a tight interplay between radiative cooling, turbulence, surface fluxes, entrainment and large scale subsidence. In the STBL, turbulence generated mainly by cloud top radiative cooling and surface fluxes, which drive the entire layer under well-mixed circumstance so that moist thermo dynamical variables below the layer are constant with height. When the STBL is shallow, typically between 400 and 800m deep, they are often well-mixed and stable. Cloud top radiative cooling and surface fluxes generate turbulent kinetic energy (TKE), which drives turbulence to mix the boundary layer; on the contrary, the large scale subsidence and boundary layer top entrainment entrain dry upper-atmosphere air into STBL, reducing turbulent kinetic energy. Although these oppose effect cancel out, the overall effect still maintains sufficient turbulence strength to well-mix the STBL when it reaches equilibrium.

However, when the turbulence is too weak to sustain the entire boundary layer under well-mixed state, STBL in the last become decoupled. STBL decoupling means the previous well-mixed layer is separated into two layers, surface fluxes driven layer (Surface-based Mixed Layer, SML) and radiative driven convection in the stratocumulus cloud layer. Between these two layers, a stable interface develops there. Cumulus clouds may
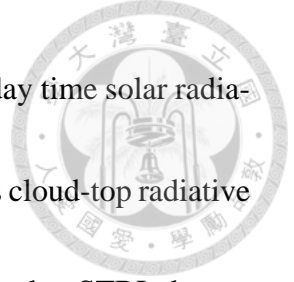
develop at the surface driven layer. Decoupling can occur when the day time solar radiation evaporates the stratocumulus cloud deck, cloud thinning and thus cloud-top radiative cooling weaken, which is the TKE source. Some other factors may lead to STBL decoupling, for example, sea surface temperature (SST) rising and drizzling. When the surface flux is too strong, it tends to form cumulus clouds below the STBL, leading to decoupling. Finally, drizzle may cause subcloud layer cooling due to drizzle evaporating.

The decoupling of STBL will cause stratocumulus dissipation due to cutting the moisture supply from sea surface. To measure the magnitude of decoupling, two common indexes are introduced: Buoyancy Integral Ratio (BIR), and Total Water mixing Ratio difference $(q_t d)$.

1.3.1   Buoyancy Integral Ratio (BIR)

Buoyancy Integral Ratio is first introduced by (Turton and Nicholls 1987), BIR is defined as the ratio between total negative buoyancy and total positive buoyancy below the boundary layer, which is:

$$BIR \equiv -\frac{\int_0^{zi} \overline{w'b'} \; dz, \; in \; which \; \overline{w'b'} < 0}{\int_0^{zi} \overline{w'b'} \; dz, \; in \; which \; \overline{w'b'} > 0} \tag{4}$$

They set BIR >0.4 as decoupled threshold yet from the observations in mid-latitude and

subtropical implies 0.17 and 0.25 for decoupling. Further refinement of BIR is conducted by (Bretherton and Wyant 1997) and (Stevens 2000). Stevens states that when BIR>0, from definition, STBL is unable to remain well-mixed; when BIR>0.10, STBL become remarkable decoupled.

1.3.2　Total water mixing ratio difference $(q_t d)$

Apart from BIR, we often use upper and lower difference of total water mixing ratio as an indicator of decoupling, which means:

$$q_t d \equiv q_t(0.25zi) - q_t(0.75zi) \tag{5}$$

Total water mixing ratio in well-mixed STBL is near constant in height. When STBL is decoupled, lower layer total water mixing ratio will increase due to sea surface moisture flux and upper layer will reduce because of lacking moisture supply from sea surface, such differences leads to higher $q_t d$. This conception is proposed by (Wood and Bretherton 2004).

From the above statement, we noticed that both BIR and $q_t d$ are subjective parameter diagnosing decoupling. BIR measure the difficulty eddies pass through the subcloud layer but it does not mean that STBL is decoupled. Because from turbulent kinetic energy budget we knows that negative buoyancy flux will simply reduce TKE, but if turbulence

9

intensity is strong enough, STBL still can maintain well-mixed state. Regarding to Total

Water Mixing Ratio difference, it quantifying the stratification within the STBL, to what

extent determine whether STBL decoupled or not depends on STBL depth, turbulence

intensity and other factors.

1.4   Adjustment time scale in STBL

1.4.1   Internal adjustment time scale

Mixed layer models have been discovered to perform two internal adjustment time

scales through calculate its eigenvalues. (Schubert et al. 1979b) used a mixed layer model

to analyze step perturbations in sea surface temperature and large-scale subsidence to

STBL. They observed that the moist thermodynamic variables (i.e., the moist static en-

ergy, h, and total water mixing ratio, q_t) adjusted with an e-folding time scales of ap-

proximately 4 h. They also found that there is a longer adjustment time scale determined

by the large-scale divergence, time scale correspond to inversion height. This behavior is

further reviewed by (Stevens 2006), he discovered that over northeast Pacific the time-

scale on which perturbations are damped, evaluates to roughly 70, 30 and 20 h for inver-

sion height, liquid-water static energy and total water mixing ratio.

1.4.2 Fast time scale adjustment (Entrainment-Liquid water Flux feed back)

(Jones et al. 2014) using simple one dimensional mixed-layer model investigate the internal response time scale for STBL. The result shows that besides the long time scale orders of 10 h to 1 days associate with boundary layer height, moist static energy and total water content, there exist a fast time scale relative to internal Entrainment-Liquid water Flux (ELF) feedback proposed by (Bretherton and Blossey 2014). When cloud is thicken due to arbitrary perturbation (i.e.: SST rising due to global warming, stated in (Bretherton and Blossey 2014)), turbulence strength enhanced through more cloud top radiative cooling, such increasing turbulence intensity leads to more vigorous entrainment at boundary layer top. This in turn causing cloud thinning to reach new equilibrium. Such negative feedback helps STBL accommodate to external forcing such as SST variation seen in Fig.3.

2. Motivation

Stratocumulus clouds experience strong diurnal variability largely due to the diurnal cycle of solar insolation. Besides the solar effect on stratocumulus variability, (Garreaud and Munoz 2004) use MM5 regional model to investigate the diurnal variation of STBL. They discover that a semi-diurnal mesoscale gravity wave formed by the interaction of the coastal jet along the Chilean coast with heating over the western Andean slopes can travel at least 1000 km over the South Eastern Pacific (here after SEP), mostly confined below 5 km, peak at 3km height. They call this wave as "upsidence" waves. Wave induced ascending motion first appears along the coast of southern Peru during afternoon, detaching from the coast by 2200 UTC (1700 LT). The horizontal wavelength is about 400 km wide and 5 km deep, phase speed is about 35 ms^{-1}, resembling to a free gravity wave in SEP region. This wave increase the amplitude of the diurnal cycles of STBL in cloud amount compare to the cycle forced by absorption of solar radiation only.

Such semi-diurnal waves is further investigated by (Rahn and Garreaud 2009). With the help of VOCALS field experiment, which provide ample data to represents the lower atmosphere features over SEP regions. They use Weather Research and Forecasting model (WRF) to study the mean state and variability of lower troposphere including circulation, STBL characteristics and the upsidence wave in SEP region. The results also

show that the simulated STBL features are relative to the southwestward propagation of an upsidence wave initiate during late evening along the Peru coast. Furthermore, they examine the different observation site data, the result show that the interference by semi-diurnal waves is clearly seen in the sounding at Iquique, influenced by a strong semi-diurnal waves compare to the radiation-driven cycle, resulting in a diurnal cycle opposite of the other sites. Although their WRF simulated STBL height is too shallow, the phase speed of upsidence wave is slower than observations, the result still highlight the importance of such waves regulating the characteristic of STBL over SEP regions. Moreover, different from previous study, such waves largely alter the diurnal cycle patterns compare to the cycle forced by absorption of solar radiation only.

(Jiang and Wang 2012) also investigate the gravity wave impact on STBL with different aerosol number concentration, they reveal that wave induced upward motion tends to increase the liquid water path and albedo. Under lower aerosol concentration, the increased LWP enhance precipitation, which in the last strengthens the mesoscale circulations in STBL, leading to cloud cellualarization. They state that in some cases, a transition from closed to open cells occurs under the influence of gravity waves, implying that some of the pockets of clouds (POCs) observed over open oceans may be related to gravity wave activities. Their study put emphasis on how upsidence wave change the mesoscale

organization of stratocumulus cloud by enhance precipitation with different CCN configurations.

Same issue is addressed by (Connolly et al. 2013), they used LES model to examine the physical mechanisms regarding to upsidence waves that cause stratocumulus mesoscale organization transition from close cell to open cell. They found that although the wave induced upward motion does cause additional drizzle formation, but this is not the main reason for the persistent reducing and changing of the cloud amount and mesoscale organization; rather it is the additional entrainment of warm aloft air into the cloud followed by the reduction in cloud top radiative cooling by reducing the cloud amount leads to the transitions. They also concern about how wave affect STBL vertical structures, which leads to irreversible changes to STBL after wave passing.

In this study, we aim to find out how such semi-diurnal wave affect STBL dynamics in more fundamental perspective using Vector Vorticity Model, namely, we only consider dynamical response to wave forcing, no solar radiation, no cloud microphysics, no precipitation to make things too complicate to analysis. Furthermore, to examine the role of entrainment liquid water flux feedback, the fast time scale adjustment first proposed by (Bretherton and Blossey 2014), what is the response of STBL under such semidiurnal upsidence wave and higher frequency wave, where the time scale resemble to ELF?

3. Methodology

As mentioned in *chapter 2*, mesoscale gravity wave in the Southeast Pacific region (SEP) is gradually gaining peoples' attention recent years.

This study first introduced mesoscale waves by adding convergence or divergence that mimics mesoscale semidiurnal waves. Method summarized as follows. Initial conditions using DYCOMS-II observation data and VOCALS cruise data are shown in Fig.3. Model environmental setting and wave strength are listed in Table.1.

Secondly, to address the issue upon ELF feedback and its fast time scale adjustment, this study conducts two set of experiments, one of them consider three hour wave period using DYCOMS-II profiles; other set following (Jiang and Wang 2012), using semi-diurnal wave period to simulate the SEP region upsidence wave with DYCOMS-II and VOCALS initial profiles, we anticipate that under shorter period of wave the STBL will not exhibit profound changes regarding to gravity waves due to ELF time scale.

Lastly, to simplify the experiments we adapt few settings: first, simulation without solar radiation, namely, consider nocturnal cases. Second, no drizzle in our simulation, limiting to dynamical changes, without any microphysical variability due to drizzle. Model used in this study, initial profiles and wave parameters, domain size issues are summarized in the following sections.

3.1 Vector Vorticity cloud resolving Model (VVM)

The cloud resolving model (CRM) used in this study was developed by (Jung and Arakawa, 2008) based on the three-dimensional anelastic vorticity equation (VVM). A unique aspect of the model is that the model predicts the horizontal components of vorticity and diagnoses the vertical velocity using a three-dimensional elliptic equation. This unique approach has an advantage at using enstrophy to diagnose the strength of mixing near inversion because in VVM vorticity is a prognostic variable, which better resolved the field variations. The physics parameterizations include a radiation parameterization using Rapid Radiative Transfer Model for GCMs (RRTMG; Iacono et al. 2008); a bulk three phase cloud microphysics parameterization including cloud droplets, ice crystals, rain, snow and graupel (Krueger et al. 1995); a surface flux parameterization (Deardorff 1972) and a first-order turbulence closure that uses eddy viscosity and diffusivity coefficients depending on deformation and stability (Shutts and Gray 1994). This model is included in a CRM intercomparison study (Fridlind et al., 2010). The results indicate that the performance of VVM is comparable to that of other CRMs. This model has also been used to study the quasi-3D multiscale modeling framework (Jung and Arakawa 2010), the topography effects on moist convection (Wu and Arakawa 2011), and the development of unified parameterization (Arakawa and Wu 2013;Wu and Arakawa 2014).

3.2 The Second Dynamics and Chemistry of Marine Stratocumulus field study (DYCOMS-II)
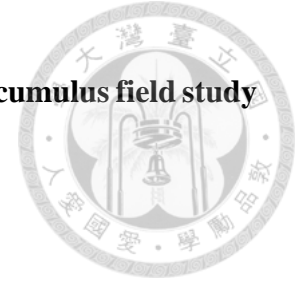
The Second Dynamics and Chemistry of Marine Stratocumulus field study (DY-COMS-II) was conducted from 7-28 July 2001 off of the coast of Southern California. DYCOMS-II was specifically designed to provide observation cases for subsequent simulation and develop entrainment parameterizations based on more accurate observation data. Of the seven nocturnal flights flown during DYCOMS-II, we use the first flight (RF01) data to serve as our initial conditions. RF01 exhibited some key features make it well suited for our study: firstly, it is nocturnal observation, which means no solar radiation enter STBL system, this help us simplify our study; the environmental conditions were relatively homogeneous; the cloud layer persisted despite the presence of mean conditions that, according to CTEI (in RF01 cases $\kappa = 0.45 > 0.23$), should have led to its dissipation; it was not complicated by the presence of significant drizzle; its energetics appeared robust to a variety of observational analyses (Stevens et al. 2005). Figure.3 shows the DYCOMS-II initial profiles used in VVM simulation, inversion height is set to 840 m, liquid potential temperature jump across inversion, $\Delta\theta_l$ is 8.5 K、$\Delta q_v = 7.5$、$\Delta q_c = 0.5$. Other parameter are summarized in Table.2

3.3 The VAMOS Ocean-Cloud-Atmosphere-Land Study (VOCALS)

The VAMOS Ocean-Cloud-Atmosphere-Land Study (VOCALS) is an international field experiment conducted since 2007 to 2008, designed to better understand physical and chemical processes vital to the climate system of the Southeast Pacific (SEP) region. The field experiment is ultimately driven by a need for improved model simulations of the coupled climate system in both the SEP and over the wider tropics and subtropics (Wood et al. 2007). VOCALS aimed to improve our understanding of the aerosol-cloud-drizzle interactions in the STBL and the physicochemical and spatiotemporal properties of aerosols; the understanding of the chemical and physical couplings between the upper ocean, the land, and the atmosphere. Specifically, one of the major goals of VOCALS is to collect intensive SEP observations and use them to compare with both regional and global coupled model simulations of the ocean heat budget, to better understand the regulation of SST and cloud cover across the SEP. The observational data used in our study is based on R/V Ronald H Brown cruise data, inversion height is set to 1100 m, $\Delta\theta_l$ is 9.5 K、$\Delta q_v = 5.5$、$\Delta q_c = 0.3$. Other parameter are also summarized in Table.2.

3.4 Mesoscale wave forcing

From the observation sounding (Rahn and Garreaud 2009), the wave is stronger than large scale subsidence in one order. Furthermore, (Garreaud and Munoz 2004) discover such gravity wave mostly confined below 5 km, intensity peak at 3km height. Wave induced ascending motion first appears along the coast of southern Peru during afternoon, detaching from the coast by 2200 UTC (1700 LT). The horizontal wavelength is about 400 km wide and 5 km deep. Therefore, we assume the horizontal and vertical wavelengths of subsidence waves are much larger than the experiment domain. This allows us to simplify the wave as:

$$D_m = D_{m0} \sin(\omega t + \phi_0) \tag{6}$$

In which, D is divergence. With the approximation above, we can introduce mesoscale upsidence wave as "horizontal homogenous wave forcing", applying to entire domain as in eq.(7), where D_0 is large scale divergence due to subsidence. The diurnal wave phase is sinusoidal seen in Fig.4.

$$\overline{w(z)} = -(D_0 + D_m)z \tag{7}$$

3.5 VVM domain size

(De Roode et al. 2004) investigates the length scale evolution with LES model quantitatively by Fourier analysis. He shows that the domain size depends on the time duration of the simulation and the type of convection. Typical stratocumulus convection the cell length is about 10 ~ 20 km. Besides the mathematical analysis, physically we can realized that if the domain size is smaller than certain convection length scales, the circulation will not being an intact pattern for such convection to grow and develop. This often leads to numerically limitation or development for clouds under arbitrary perturbations.

In this study, we have examined small domain size under wave forcing. The result reveals that when adapt small domain ($\mathbf{3.2\ km \times 3.2\ km}$), the clouds almost disappear after $\mathbf{5_{th}}$ hours even in the free run simulations, no perturbation being added into. To avoid such numerically limitation for clouds development, we use $\mathbf{25.6\ km \times 25.6\ km}$ in upsidence waves run and $\mathbf{12.8\ km \times 12.8\ km}$ in high frequency waves run. Those larger domain sizes allow cloud cells to grow over the 12 hours simulations. The results in free run simulations show that this domain size is suitable for this study, the cloud cell size keep growing over time. At the end of the experiment, this domain size can cover one to four intact cloud cells to develop.

4. Results and Analysis

4.1 High frequency waves

In the first part of the experiments, the study aim to examine the STBL response under higher frequency gravity waves: the time scale resemble to the entrainment liquid flux feedback, namely, the fast time scale adjustment proposed by (Bretherton and Blossey 2014). To achieve this, the three hour period wave, as is depicted in Fig.4, is imposed to the experiment domain homogeneously.

First of all, the inversion height is derived from cloud water mixing ratio, in this study the vertical resolution is about 10m at lower layer, it is not sufficient to resolve the entrainment interface layer so that inversion height is calculate directly from cloud water, not far from maximum-gradient height or turbulent mixing maximum height. The result from Fig.5 indicates that no significant changes after wave passing, inversion height remain the same when the wave undergoes a cycle at 03,06,09 and 12Z, although at 12Z it become slightly lower than control run; in addition to the mean value trend, shading represent a stranded deviation from mean value, it reveals that at the wave induced upward motion phase, the horizontal variability reduced; at the induced downward motion phase, the variability increased.

The evolution of inversion height is relative to subsidence and entrainment velocity;

further, the entrainment velocity is derived from the vertical structure of STBL. We also

examine the vertical profile of cloud water mixing ratio and potential temperature at the

end of the experiment, they both remain largely unchanged. After wave passing the cloud

layer become slightly thicker, cloud base do not changes and cloud top increased, but the

concentration decreased. As for potential temperature changes, it merely shows no differ-

ence between two runs except somewhat higher inversion height.

Even though at the end of the experiment the albedo become slightly lower, the ver-

tical structure of potential temperature and cloud water mixing ratio showing no notable

structural differences, this study further inspect the vertical structure variations quantita-

tively using the decoupling index Buoyancy Integral Ratio(BIR) and Total water mixing

ratio difference($q_t d$) introduced in *Chapter 1.3*. The result seen in Fig.6 and Fig.7 still

indicate there is no significant vertical structure changes, precisely the decoupling mag-

nitude.

Summary

First part of the experiments examines the STBL response under horizontally homogenous three hour period waves to address the STBL fast time adjustment issue. Presumably, STBL may not be affect by such waves because the time scale of waves is comparable to ELF feedback, which means when wave perturb the cloud deck, ELF start adjusting. But before the adjustment accommodate the perturbation, wave have already passed through so that for STBL it did not significantly experiencing the wave perturbation.

The result agree with the presumption very well, first of all, the cloud field shows that no significant changes after wave passing compare to control run; furthermore, the vertical structures remain the same as is in control run; lastly from quantitatively view, despite exhibit more different trend compare to control run, BIR and $q_t d$ indicate no decoupling happens after wave passing. The only deviation observed is that cloud deck grow into more horizontally homogeneous and mildly smaller albedo.

4.2 Semi-diurnal Waves

In the second parts of the experiments, we present two set of the simulations with different initial profiles and lower boundary conditions, which is DYCOMS-II RF01 Flight data and VOCALS cruise data to investigate the response under semi-diurnal waves. Overall, the wave induced variation of vertical velocities may increase the large scale subsidence or decrease the subsidence. Therefore, in semi-diurnal waves experiments we separate the timeline into two regimes: *regime I* and *regime II,* reflect the different effect toward subsidence strength.

First of all, Fig.8 illustrates the domain average of time series and domain snapshots of pseudo albedo, blue line is the DYCOMS-II simulation, Orange line is the VOCALS simulation. We observe that the cloud in the upsidence wave run become thicker and exhibit more horizontal homogeneity when wave impose an updraft in *regime I*. In contrast, when negative phase induced downdraft in *regime II*, such downdraft bringing warm air aloft into STBL so that warm the STBL, dry out the cloud decks, resulting in the dissipation of cloud decks and more heterogeneity in the domain. Same result seen in the time series of pseudo albedo. In the *regime I*, wave induced updraft promote thicker clouds, hence exhibit higher albedo; in *regime II*, wave induced downdraft result in smaller cloud coverage so that the albedo reduced to about 0.3.

The inversion height is also derived from cloud water mixing ratio. The result from Fig.9 reveals that after wave passing, the inversion height shows a peak value near 6th hour, this is reasonable due to the sinusoidal wave pattern imposed in the domain; nevertheless, at the end of the experiment it become lower than control run. This height response is mainly due to the STBL decoupling (further investigations refer to Appendix A). In addition to the mean value trend, shading represent a stranded deviation from mean value, similarly, it reveals that at the wave induced upward motion phase, the horizontal variability reduced; at the induced downward motion phase, the variability increased, consistent with pseudo albedo snapshots in Fig.8

Further examine the response under semi-diurnal waves. Fig. 10 and Fig.11 represent the vertical structures of cloud water mixing ratio, and total water mixing ratio at the start and the end of the experiments. Fig.10 shows the cloud water profile, indicating after wave forcing the cloud mixing ratio become more diluted particularly near cloud top and experiencing lower cloud top height. As for temperature profiles, even though it seems presenting two layer structures, it is not very remarkable; however, in Fig.11, total water mixing ratio profile shows significant two layer structures in the middle of the STBL.

This two layer result indicate the STBL is become decoupled after impose semi-diurnal waves. To gain insight into the structural changes, we also inspect the vertical

profile of Cloud Water mixing ratio at the 3rd experiment hour and 09 Z, which helps us

reveal the spatial variability and vertical structure changes. Fig.12 shows the cloud water

profile at 3rd hours, where the wave induced updraft is the greatest, wave run exhibit flat

cloud base and thicker, denser cloud compare to control run albeit no notable vertical

structure differences. Nevertheless in Fig.13, at 09Z the STBL experiencing profound

changes, clouds become more cumuliform, thickness reduced, and distinctively, the two

apart cloud layer are observed, tally with the two layer structure shown in Fig.11.

To further investigate the vertical structure variations quantitatively, we calculate the

decoupling index Buoyancy Integral Ratio (BIR) and Total Water mixing ratio difference

($q_t d$) introduced in *Chapter 1.3*. Fig.14 demonstrates the BIR index over time, both run

are smoothed by three point moving average for clarity, shading represents the BIR crite-

rion for decoupling. As is mentioned in *Chapter 1.3*, although for those index the criterion

are subject, in here we following (Stevens 2000), which stated that when BIR > 0.10, the

STBL exhibit more significant decoupling. Fig.14 shows that control run remain about

0.03 over time; on the contrary, waves run exhibit larger perturbation. Both simulations

the BIR is increased in *regime I* and is decreased in *regime II*. From the shading we can

infer that at 04:30Z the STBL become decoupled in DYCOMS-II, 05Z in VOCALS sim-

ulations. Similar results shown in Fig.15. In *regime I*, the $q_t d$ value in wave run is

smaller than control run; however, in *regime II* it increase at later moment. Both parame-

ters reveal that STBL is decoupled at the end of *regime I.* Furthermore, in DYCOMS-II

simulation the $q_t d$ at 09 Z~10 Z it slightly recovered. This is somewhat weird but note-

worthy and we will further investigate in later.

Summary

Second part of the experiments examines the STBL response under semidiurnal upsidence waves. Presumably, STBL will be greatly impacted by such waves because the time scale of waves are much longer than ELF feedback, which means when wave perturb the cloud deck, ELF start adjusting but owing to the shorter time scale of ELF feedback compare to upsidence wave, the cloud field will experience significant alteration through the adjustment process.

The result still coincide with the presumption very well, first of all, the cloud field shows that after wave passing the cloud deck greatly dissipated; furthermore, there is a remarkable two layer structure observed in total water mixing ratio profiles and cloud water mixing ratio slices; lastly from quantitatively view, wave runs evolved into decoupled structures at about 04:30Z in DYCOMS-II and 05:30Z in VOCALS simulations, both indicate that the wave induced decoupling is happened in the *regime I*. Also, in DYCOMS-II simulations the BIR index shows earlier decoupling than $q_t d$ index. Even though the result coincide with the presumption very well, there still rise some interesting issue that in next section we are going to delved into.

4.3   Analysis—STBL decoupling in *Regime I*

Why in DYCOMS-II run the identified timing of decoupling by BIR is earlier than

$q_t d$ but in VOCALS run it is about the same time? From the results, we notice there is a

disparity between DYCOMS-II and VOCALS simulations about the identified timing of

two decoupling indexes. To answer this question, we first examine how STBL evolved

into decoupled structures by (Bretherton and Wyant 1997) and (Bretherton and Blossey
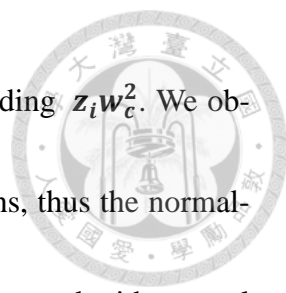
2014).

4.3.1   How STBL evolved into decoupled structure?

First of all, by (Bretherton and Wyant 1997), the cloud base jump is proportional to

vertical moisture transport, namely, vertical total water flux; further, under zero surface

flux condition, such cloud base buoyancy jump is just proportional to cloud thickness, so

called deepening warming decoupling. Furthermore, from (Bretherton and Blossey 2014),

when cloud is thicken due to arbitrary perturbation, turbulence strength will be enhanced

through exhibit more cloud top radiative cooling, such increasing turbulence intensity

leading to more vigorous entrainment at boundary layer top and this in turn, causing cloud

thinning to adjust to new equilibrium, which is the ELF feedback.

In our case, these two mechanism cause STBL decoupled before wave induced

downdraft warms STBL, forming a stable layer within STBL. When cloud deck is thicken

due to the wave induced updraft as seen in Fig.12. The Entrainment Liquid water Flux

feedback start adjusting STBL to reach new equilibrium; on the other hand, when clouds

thicken, the buoyancy flux jump increased because of larger latent heat release in the

thicken cloud layer, forming a negative buoyancy flux layer at the cloud base. These two

mechanism actually served as the same role through Liquid water flux in regulating the

cloud field perturbation. That is, when cloud is thicken due to arbitrary forcing, such

larger LWP promoting more TKE by cloud top radiative cooling which in turn drive more

vigorous cloud top entrainment; similarly, such thicken cloud also promote a larger cloud

base buoyancy jump, which is the negative buoyancy flux at cloud base, those two process

both leads to weaken the TKE to reduce the cloud thickness, reaching new equilibrium

by different means: entrain more dry air into STBL or exhibit a TKE sink layer within

STBL. Even though ELF feedback and cloud base buoyancy jump served as the regulat-

ing role, in the upsidence wave case, it will lead to STBL decoupling. ELF feedback plus

cloud base buoyancy jump reduce TKE so that in the last the turbulence strength is too

weak to sustain the well-mixed STBL before the wave induced downdraft warm the STBL,

causing warming decoupling. Fig.16 shows the turbulence strength by calculate the ver-

tical integrated TKE, but in our simulation the inversion height is varying over time, to

compare with control run, we normalize the Integrated TKE by dividing $z_i w_c^2$. We observed in *Regime I,* where wave induced updraft cause cloud thickens, thus the normalized ITKE first increased; however, after 03Z it start decreasing compared with control run. This decreasing in accordance with previous mentioned adjustment, further shown in Fig.18a, Fig.18b, when cloud thickens the cloud base buoyancy jump increased, in DYCOMS-II case, about at 04Z it shows negative buoyancy flux at cloud base; in VOCALS case it appear later about 05Z to 06Z,due to the weaker surface flux. Also, from the vertical total water flux is shows about the same time it exhibit larger jump at cloud base level. Both earlier appeared adjustment make TKE become too weak to sustain well-mixed STBL so in the last it become decoupled, as index shown in Fig.14 and Fig.15.

To sum up, those evidence shows that when cloud thickened by waves, the ELF feedback and cloud base buoyancy jump start adjusting to thinning the cloud but in the last leads to the STBL decoupling before the wave induced downdraft bringing warm aloft air into STBL cause warming decoupling.

4.3.2 Turbulence intensity, inversion height and decoupling

Although the result in DYCOMS-II and VOCALS both showing the STBL eventually become decoupled for a given upsidence wave forcing. Before further study two simulations, we first examine the physical meaning of two distinct decoupling index: BIR

31

and $q_t d$. Recall from *Chapter 1.3,* Buoyancy Integral Ratio measures the relative portion of negative buoyancy flux area within STBL, this implicate that BIR diagnose the decoupling based on turbulent energetic concern. From TKE equation, we know that buoyancy flux served as a TKE sourcing term in TKE equation. BIR measure the difficulty eddies pass through the subcloud layer, if BIR is large, eddies passing through such layer will reduce TKE; however if turbulence intensity is strong enough, STBL can still maintain well-mixed state, to what extent determine whether STBL decoupled or not depends on STBL depth and turbulence intensity. Regarding to Total Water Mixing Ratio difference $q_t d$, differ from BIR, it measures the stratification within the STBL so it truly reflect the strength of the stable layer formed in the middle of the STBL when it became decoupled.

Hence, if there exist two STBL that one is shallower, we anticipate the decoupling timing difference between BIR and $q_t d$ will larger in the shallower ones because even though BIR diagnose STBL as decoupled, the shallower PBL depth is easier for turbulence to maintain well-mixed state if turbulence intensity between two STBL are about the same.

Fig.14 shows the Time series of buoyancy integral ratio (BIR) and Fig.15 shows the Total Water difference ($q_t d$), we can clearly observe that the decoupled timing between

BIR and $q_t d$ is larger in DYCOMS-II. BIR is about 04:30 Z; however $q_t d$ is about

05:30 Z, note that in here we assume when $q_t d$ in wave run is larger than control run,

the STBL is diagnosed as decoupled. In contrast, the BIR and $q_t d$ diagnosed decoupling

time is about the same. Even though in VOCALS run it exhibit stronger turbulence inten-

sity at 04 Z to 06 Z, shown in Fig.16.

Other possibility that may produce earlier BIR diagnosed decoupling is the stronger

surface flux, such stronger surface flux may favor the cumuliform cloud formed below

the cloud decks and cause decoupling, one can see this phenomenon in Fig18a, 18b,

stronger surface flux produce larger cloud base buoyancy flux jump. From the Fig 15, we

can also observe such effect of stronger surface flux, resulting in pre-exist weak stratifi-

cation within STBL in DYCOMS-II simulation.

4.4   Analysis—Cloud coverage response in *Regime II*

In the last section, we aim to figure out why there exist such discrepancy of the response between two initial profiles in *Regime II*.

First of all, we examine the vertical profile difference. The STBL temperature is warmer in VOCALS, and the water vapor mixing ratio in STBL is smaller also in VOCALS. From the inversion jump value, DYCOMS-II profiles is dryer at free atmosphere so that the κ is larger (and > 0.23) than VOCALS profiles. This infer that in DYCOMS-II the cloud is more likely to dissipate by Cloud Top Entrainment Instability, where dry aloft air mixed into cloudy air cause cloud evaporate and in the last the evaporative cooling of cloud water generate colder air from environment thus produce TKE, in the last leads to further cloud dissipating. However, the results show that VOCALS cloud layer greatly dissipated instead of DYCOMS-II at the end of the experiment. So the reason why exist such cloud coverage discrepancy may not reside in CTEI mechanism.

To further investigate the reason why in VOCALS simulation the cloud greatly dissipated, we turning back examine the cloud water profile in Fig.13. It seems that in VOCALS simulation the cloud forming at the top of surface-based mixed layer (SML) is less than in the DYCOMS-II simulation. To further verify this difference, Fig.19 shows the time series of cloud fraction in both simulations. The shading scale and color is set to

uneven scales and transparent to put emphasis on the difference of cumulus cloud fraction, note that in DYCOMS-II simulation the cloud fraction is larger than in VOCALS. To further examine the cloud fraction differences, we calculate the cloud fraction at certain level of normalized height, namely, the subcloud level: $z/z_i = 0.65\sim0.7$. The result shows that in DYCOMS-II the cloud fraction at the top of the surface-based mixed layer is about $4\sim5\%$, yet in VOCALS simulation is almost remain below 1%.

This larger area of surface-based mixed layer cumuliform cloud may help STBL stay their cloud decks under wave forcing by the intermittently coupling with the upper stratocumulus decks. Such mechanism is first proposed by (Martin et al.; Wang and Lenschow 1995) that the surface-based mixed layer formed clouds produce convergent flow in the lower mixed layer and thus compensating diverging flow in the upper mixed layer, identified along the flight track of ASTEX field experiment. This flow field, not only locally supply moisture from sea surface but also further helps to transport moisture upwards from the sea surface and disperse into the surrounding cloud decks, thus helping maintain the stratocumulus clouds.

Since from the above discussion we cannot certainly point out such cloud faction is contributed by SML cumulus clouds and also, we notice from Fig.15 that at 09 Z~10 Z the stratification is weakened in DYCOMS-II while in VOCALS it remain the same.

Therefore, to verify the cumulus activity difference we conduct the mass flux analysis and inspect turbulent profiles at 07 Z~10 Z.

Firstly, the surface flux affect the STBL structure and thus the formation of SML clouds. Fig.21 shows the mass flux at LCL height, which represent the cumulus activity, the brown line is the VOCALS simulation, and dark blue line is DYCOMS-II simulation. To further inspect the DYCOMS-II evolution itself, the transparent dark blue line represents the mass flux at last hour. It shows that at 07 Z two simulations the mass flux are near identical and also we can see the updraft mass flux is spread to higher velocity bins, yet the downdraft features large fraction of weak vertical velocity, this is the typical cumuliform clouds mass flux pattern. Even though at 07 Z two simulations are similar, at 08 Z we observed that in VOCALS simulation the mass flux is significantly reduced compare to DYCOMS-II. Also, the updraft mass flux at higher velocity bins is greatly reduced and increased at lower velocity bins, which means the cumulus activity is suppressed compare to DYCOMS-II simulations. In contrast, in the DYCOMS-II the updraft mass flux still maintain some intensity over the time, which illustrate the higher cumulus clouds occurrence.

To further confirm the cumulus clouds activity difference in two simulations, we also examine the buoyancy flux profiles and vertical cloud water flux profiles at 07 Z~10

Z. In fig.22, upper panel shows buoyancy flux in two simulations at 07 Z~10 Z, lower panel indicates the vertical cloud water flux in two simulations at 07 Z~10 Z. From buoyancy flux we observe that in VOCALS simulation the buoyancy flux in cloud region significantly reduced over the time but patterns remain the same as previous shown buoyancy flux at 04 Z~ 06 Z in Fig.18, which means in VOCALS the cloud dissipate over time so that the positive region of buoyancy flux in cloud layer reduced but the low occurrence of cumulus cloud did not affect the structure of STBL in turbulent energetic view; on the contrary, in DYCOMS-II we can clearly notice over the time the buoyancy in the cloud layer do reduced due to upsidence waves and STBL decoupling. However, we also observe that the subcloud layer exhibit larger positive value so that in the buoyancy flux profile the positive area become vertically broader, such positive buoyancy flux at subcloud layer represents the cumulus structural influence on STBL. Likewise, vertical cloud water flux profiles shows that DYCOMS-II simulation exhibit broader distribution at subcloud level compare to VOCALS simulation. These two profiles agree with the mass flux evolution at LCL height, inferring that in DYCOMS-II simulation the cumulus clouds are more active than in VOCALS simulation.

From the above discussion we realized that the surface-based mixed layer clouds

helps maintain the upper stratocumulus cloud decks under wave forcing and thus contrib-

ute to the different response between DYCOMS-II and VOCALS simulations. Then the

next question comes to what factors in VOACLS simulation inhibit the formation of sur-

face-based mixed layer clouds? Firstly, from the conceptual models of the formation of

stratocumulus, we know that the cloud formed above the surface Lifting Condensation

Level (LCL) under well-mixed STBL. How is the surface-based mixed layer cloud

formed? When the STBL decoupled, the upper and lower layer water vapor difference is

enlarge over time: the upper layer the water vapor is reduced due to the cut off of moisture

supply from sea surface; on the contrary, the lower layer, namely the surface-based mixed

layer, water vapor is increased. Thus the surface LCL is lowered so that the surface-based

mixed layer clouds formed. Fig.17 shows how the lower layer water vapor is built after

the STBL is decoupled, and one can observe that in VOCALS simulation the lower layer

water vapor growth rate is slower than in DYCOMS-II simulation due to the weaker pre-

scribed sea surface fluxes, seen in the Fig.18a, 18b of the near surface $w'b'$ and $w'q_t'$.

Also, from the mass flux analysis it shows that higher surface fluxes promote stronger

updraft after STBL decoupled. We thought these two effects of sea surface fluxes are the

main reason contribute to such weaker SML cumuliform clouds and thus in the last greatly

dissipation of upper layer stratocumulus clouds. When STBL decoupled, the stronger sea

38

surface fluxes helps building up the lower layer water vapor, thus lowering the LCL so

that the cumuliform cloud is easier to form beneath the upper stratocumulus cloud decks.

Fig.17 shows at 06Z~09Z the lower layer water vapor remain within the range of 8.0~8.1

in VOCALS; 8.9 to 9.2 in DYCOMS-II. This may help lower the LCL so that surface-

based mixed layer clouds can be formed easier, it is shown in Fig.20 that in DYCOMS-II

the LCL is significant lower than SML.

Apart from the weaker sea surface flux, the higher inversion height may also make

the formation of surface-based mixed layer clouds harder. For fixed turbulence intensity,

it is harder for STBL or SML while retain well-mixed state. Therefore under weaker sur-

face flux and higher PBL height like the VOCALS simulation, the SML cloud won't form

as easily as in DYCOMS-II simulation.

In conclusion, the different cloud coverage response observed between DYCOMS-

II and VOCALS simulations may attribute to the different occurrence of SML cumulus

clouds. According to (Wang and Lenschow 1995), the presence of Surface-based Mixed

Layer (SML) formed clouds helps maintain upper layer clouds by intermittent coupling

two layer, transporting sea surface moisture into upper layer clouds, producing secondary

circulation to spread out the moisture into surrounding. Moreover, the different occur-

rence of sub mixed layer clouds may due to the sea surface flux difference and the PBL

height difference, which determine the low level updraft strength and how hard the air

parcel travel through Surface-based Mixed Layer. Under weaker surface flux, the decou-

pled STBL exhibit lower updraft mass flux and cannot build up lower layer water vapor

easily to lowering LCL significantly, forming the SML clouds easier.
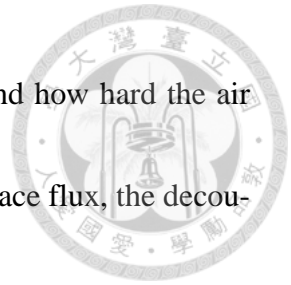
5. Conclusion and future work

5.1 Conclusion

This study use Vector Vorticity Model (VVM) to simulate the upsidence wave impact on Stratocumulus-Topped Boundary Layer (STBL). Also, to address the issue of Entrainment-Liquid water Flux Feedback (ELF feedback), namely the fast time scale adjustment first proposed by (Bretherton and Blossey 2014), we set up two set of the experiments, one of them imposed horizontal homogenously three hour high frequency wave forcing; the other imposed semi-diurnal waves to mimic the upsidence waves observed over SEP region by (Garreaud and Munoz 2004). This study further investigate the STBL response under upsidence waves in different initial conditions. We consider two distinct initial profiles coming from DYCOMS-II and VOCALS regional field observations. In DYCOMS-II the PBL is shallower, the cloud is m and presents stronger sea surface flux especially the moisture flux compared to VOCALS profiles.

In the first part of the experiments, the high frequency waves run shows no significant response compared to control run. At the end of the experiments, the cloud field shows that no significant changes after wave passing compare to control run; furthermore, the vertical structures remain the same as is in control run; lastly from quantitatively view,

despite exhibit more different trend compare to control run, BIR and q_{td} indicate no decoupling happens after wave passing.

In the second part of the experiments, we examine the STBL response under upsidence waves and different initial conditions.

From the holistic result, it shows that at the end of the experiments, the cloud coverage greatly reduced compare to control run; furthermore, there is a remarkable two layer structure observed: upper stratocumulus layer and Surface-based Mixed Layer (SML) in total water mixing ratio profiles and cloud water mixing ratio profiles, which means the STBL is decoupled. From quantitatively view, wave runs evolved into decoupled structures at about 04:30Z in DYCOMS-II and about 05:30Z in VOCALS simulations from BIR index, both indicate that the wave induced decoupling is happened before the negative phase of the waves. The ELF feedback plus the cloud base buoyancy jump contribute to the STBL decoupling.

Further, this study compare two set of the simulations under semi-diurnal waves. We observed that in the DYCOMS-II simulation, the BIR identified decoupling time is earlier than q_{td} identified; but in VOCALS simulation it is about the same timing. Such different response may owing to the PBL height and turbulence intensity. It is easier for weaker turbulence strength and deeper STBL to become decoupled and thus the BIR and q_{td}

identified decoupling time will closer.

In addition, we investigate the different response of cloud coverage in *Regime II*. Such difference is due to the occurrence of SML clouds, which helps transport the sea surface moisture into decoupled upper layer thus maintain the cloud coverage. The formation of SML clouds can also be realized by the conceptual model of stratocumulus formation introduced by Houze. When the STBL decoupled, the lower layer water vapor increased due to the sea surface flux, surface flux helps lower layer building up the water vapor so that the LCL height drop down till the height near SML level, the SML clouds formed. Thus we can observed that in DYCOMS-II simulation the stronger surface flux helps STBL maintain its cloud decks under upsidence waves by higher occurrence of surface-based mixed layer clouds.

In a nut shell, the stronger sea surface flux yet can contribute to STBL decoupling, it helps decoupled STBL maintain the upper layer stratocumulus clouds by promote more surface-based mixed layer clouds thus transporting moisture upward into the upper layer, helping sustaining the stratocumulus clouds.

Our result highlight the importance of the upper free atmosphere perturbations like semi-diurnal waves. The physical process within the STBL has been the focus of a great deal of research in the last decades. This study shows such free atmosphere perturbations

may largely impact the STBL structures through altering the strength of large scale subsidence. We focus on how such semi-diurnal waves affect stratocumulus off the coast of California and South Eastern Pacific (SEP) regions. The results show that STBL decoupled and eventually the albedo drop from 0.7 to below 0.3 in both regions. Such response may not resolved by (Garreaud and Munoz 2004) and (Rahn and Garreaud 2009), which use WRF regional model to investigate the STBL variability near SEP region.

5.2 Future work

From the last part of the result, we speculate that the surface flux strength difference contribute to the different response in two simulations by forming SML cumulus clouds. However, those two profiles we used as initial conditions are not only different in surface fluxes strength but also the inversion depth, inversion jump value and thus the κ. In this study we focus on how such semi-diurnal waves affect stratocumulus off the coast of California and South Eastern Pacific (SEP) regions. The result shows it may cause STBL decoupled and both region may exhibit different response. However, to further study the different response after STBL decoupled under perturbations, we have to separate some variables systematically to examine how surface flux affect such response while fixing PBL height and inversion jump values.

Also, in the *Regime II* of inversion height, we observed that two profiles exhibit

different horizontal variability, it may relative to the κ. With the larger κ as is in DY-

COMS-II, the free atmospheric perturbation may enhance the eddy activity near the in-

version. To investigate the κ and its influence with free atmospheric perturbations on

STBL, we have to use single profiles and lower boundary conditions and change the jump

value.

Furthermore, in this study we did not consider how microphysical process influence

STBL structures yet resent study most focus on how these microphysical process affect

STBL on mesoscale organization since waves induce updraft promote drizzling. We an-

ticipate that STBL will still decoupled in *Regime I* with mechanism different from this

study (may caused by drizzle). Nevertheless, the response in *Regime II* may complicated.

Further investigation including microphysical scheme regarding to mesoscale waves is

needed.

To sum up, there are three sets of the experiment to investigate the STBL response

under wave forcing:

Experiment I: Fix inversion jump value, single profiles with different surface fluxes

$\Rightarrow$ With surface flux being $\quad 0, 30.6, 100, \mathrm{W/m^2}$

Experiment II: Fix surface fluxes, single profiles with different inversion jump value
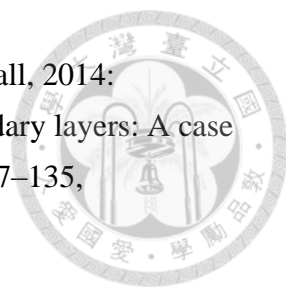
$\Rightarrow$ With κ being $\quad \ll 0.23, \sim 0.23, \gg 0.23$
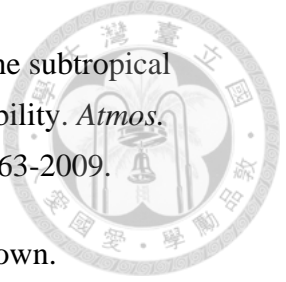
Experiment III: Same configuration in this study but with microphysics, promoting the

drizzle event.

References

Arakawa, A., and W. H. Schubert, 1974: Interaction of a cumulus cloud ensemble with the large scale environment, {P}art {I}. *J. Atmos. Sci.*, **31**, 674–701, doi:10.1175/1520-0469(1974)031<0674:IOACCE>2.0.CO;2.

Arakawa, A., and C.-M. Wu, 2013: A Unified Representation of Deep Moist Convection in Numerical Modeling of the Atmosphere. Part I. *J. Atmos. Sci.*, **70**, 1977–1992, doi:10.1175/JAS-D-12-0330.1. http://journals.ametsoc.org/doi/abs/10.1175/JAS-D-12-0330.1.

Bretherton, C. S., and M. C. Wyant, 1997: Moisture Transport, Lower-Tropospheric Stability, and Decoupling of Cloud-Topped Boundary Layers. *J. Atmos. Sci.*, **54**, 148–167, doi:10.1175/1520-0469(1997)054<0148:MTLTSA>2.0.CO;2.

——, and P. N. Blossey, 2014: Low cloud reduction in a greenhouse-warmed climate: Results from Lagrangian les of a subtropical marine cloudiness transition. *J. Adv. Model. Earth Syst.*, **6**, 91–114, doi:10.1002/2013MS000250.

Connolly, P. J., G. Vaughan, P. Cook, G. Allen, H. Coe, T. W. Choularton, C. Dearden, and a. Hill, 2013: Modelling the effects of gravity waves on stratocumulus clouds observed during VOCALS-UK. *Atmos. Chem. Phys.*, **13**, 7133–7152, doi:10.5194/acp-13-7133-2013. http://www.atmos-chem-phys.net/13/7133/2013/.

Deardorff, J. W., 1972: Parameterization of the planetary boundary layer for use in general circulation models. *Mon. Weather Rev.*, **100**, 93–106, doi:10.1175/1520-0493(1972)100<0093:POTPBL>2.3.CO;2.

Fridlind, A., A. Ackerman, J. Petch, and P. F., 2015: ARM / GCSS / SPARC TWP-ICE NWP Intercomparison Study ARM / GCSS / SPARC TWP-ICE NWP Intercomparison Study.

Garreaud, R. D., and R. Munoz, 2004: The diurnal cycle in circulation and cloudiness over the subtropical southeast Pacific: A modeling study. *J. Clim.*, **17**, 1699–1710, doi:10.1175/1520-0442(2004)017<1699:TDCICA>2.0.CO;2.

Ghate, V. P., B. a. Albrecht, M. a. Miller, A. Brewer, and C. W. Fairall, 2014: Turbulence and radiation in stratocumulus-topped marine boundary layers: A case study from VOCALS-REx. *J. Appl. Meteorol. Climatol.*, **53**, 117–135, doi:10.1175/JAMC-D-12-0225.1.

Iacono, M. J., J. S. Delamere, E. J. Mlawer, M. W. Shephard, S. a. Clough, and W. D. Collins, 2008: Radiative forcing by long-lived greenhouse gases: Calculations with the AER radiative transfer models. *J. Geophys. Res. Atmos.*, **113**, 1–8, doi:10.1029/2008JD009944.

Jiang, Q., and S. Wang, 2012: Impact of Gravity Waves on Marine Stratocumulus Variability. *J. Atmos. Sci.*, 120802091525000, doi:10.1175/JAS-D-12-0135.1.

Jones, C., C. Bretherton, and P. Blossey, 2014: Fast stratocumulus time scale in mixed layer model and large eddy simulation. *J. Adv. Model. Earth Syst.*, 1–17, doi:10.1002/2013MS000289.Received. http://onlinelibrary.wiley.com/doi/10.1002/2013MS000289/abstract.

Jung, J.-H., and A. Arakawa, 2010: Development of a quasi-3D multiscale modeling framework: Motivation, basic algorithm and preliminary results. *J. Adv. Model. Earth Syst.*, **2**, doi:10.3894/JAMES.2010.2.11.

Krueger, S. K., Q. Fu, K. N. Liou, and H.-N. S. Chin, 1995: Improvements of an ice-phase microphysics parameterization for use in numerical simulations of tropical convection. doi:10.1175/1520-0450-34.1.281.

Kuo, H.-C., and W. H. Schubert, 1988: Stability of cloud-topped boundary layers. *Q. J. R. Meteorol. Soc.*, **114**, 887–916, doi:10.1002/qj.49711448204. http://doi.wiley.com/10.1002/qj.49711448204.

Lilly, D., 1968: Models of cloud-topped mixed layers under a strong inversion. *Q. J. R. Meteorol. Soc.*, **94**, 292–309, doi:10.1002/qj.49709440106. http://onlinelibrary.wiley.com/doi/10.1002/qj.49709440106/abstract.

Martin, G. M., D. W. Johnson, D. P. Rogers, P. R. Jonas, P. Minnis, and D. A. Hegg, 1995: Observations of the Interaction between Cumulus Clouds and Warm Stratocumulus Clouds in the Marine Boundary Layer during ASTEX. *J. Atmos. Sci.*, **52**, 2902–2922, doi:10.1175/1520-0469(1995)052<2902:OOTIBC>2.0.CO;2.

Rahn, D. a., and R. D. Garreaud, 2009: Marine boundary layer over the subtropical southeast Pacific during VOCALS-REx – Part 2: Synoptic variability. *Atmos. Chem. Phys. Discuss.*, **9**, 26063–26094, doi:10.5194/acpd-9-26063-2009.

Randall, D. a., 1980: Conditional instability of the first kind upside-down. doi:10.1175/1520-0469(1980)037<0125:CIOTFK>2.0.CO;2.

De Roode, S. R., P. G. Duynkerke, and H. J. J. Jonker, 2004: Large-Eddy Simulation: How Large is Large Enough? *J. Atmos. Sci.*, **61**, 403–421, doi:10.1175/1520-0469(2004)061<0403:LSHLIL>2.0.CO;2.

Schubert, W. H., J. S. Wakefield, E. J. Steiner, and S. K. Cox, 1979a: Marine Stratocumulus Convection. Part I: Governing Equations and Horizontally Homogeneous Solutions. *J. Atmos. Sci.*, **36**, 1286–1307, doi:10.1175/1520-0469(1979)036<1286:MSCPIG>2.0.CO;2. http://journals.ametsoc.org/doi/abs/10.1175/1520-0469(1979)036<1286:MSCPIG>2.0.CO;2.

——, ——, ——, and ——, 1979b: Marine Stratocumulus Convection. part II: Horizontally Inhomogeneous Solutions. *J. Atmos. Sci.*, **36**, 1308–1324, doi:10.1175/1520-0469(1979)036<1308:MSCPIH>2.0.CO;2.

Shutts, G. J., and M. E. B. Gray, 1994: A numerical modelling study of the geostrophic adjustment process following deep convection. *Q. J. R. Meteorol. Soc.*, **120**, 1145–1178, doi:10.1002/qj.49712051903. http://doi.wiley.com/10.1002/qj.49712051903.

Stevens, B., 2000: Cloud transitions and decoupling in shear-free stratocumulus-topped boundary layers. *Geophys. Res. Lett.*, **27**, 2557–2560, doi:10.1029/1999GL011257.

Stevens, B., 2006: Bulk boundary-layer concepts for simplified models of tropical dynamics. *Theor. Comput. Fluid Dyn.*, **20**, 279–304, doi:10.1007/s00162-006-0032-z.

——, and Coauthors, 2005: Evaluation of Large-Eddy Simulations via Observations of Nocturnal Marine Stratocumulus. *Mon. Weather Rev.*, **133**, 1443–1462, doi:10.1175/MWR2930.1.

Turton, J. D., and S. Nicholls, 1987: A Study of the Diurnal Variation of Stratocumulus Using A Multiple Mixed Layer Model. *Q. J. R. Meteorol. Soc.*, **113**, 969–1009, doi:10.1002/qj.49711347712. http://dx.doi.org/10.1002/qj.49711347712.

Wang, Q., and D. H. Lenschow, 1995: An Observational Study of the Role of Penetrating Cumulus in a Marine Stratocumulus-Topped Boundary Layer. *J. Atmos. Sci.*, **52**, 2778–2787, doi:10.1175/1520-0469(1995)052<2778:AOSOTR>2.0.CO;2.

Wilhelmson, R. B., and C.-S. Chen, 1982: A Simulation of the Development of Successive Cells Along a Cold Outflow Boundary. *J. Atmos. Sci.*, **39**, 1466–1483, doi:10.1175/1520-0469(1982)039<1466:ASOTDO>2.0.CO;2.

Wood, R., and C. S. Bretherton, 2004: Boundary layer depth, entrainment, and decoupling in the cloud-capped subtropical and tropical marine boundary layer. *J. Clim.*, **17**, 3576–3588, doi:10.1175/1520-0442(2004)017<3576:BLDEAD>2.0.CO;2.

Wood, R., C. S. Bretherton, B. Huebert, C. R. Mechoso, and R. Weller, 2007: The VAMOS Ocean-Cloud-Atmospher-Land Study: Program Summary. *Program*,.

Wu, C. M., and A. Arakawa, 2011: Inclusion of surface topography into the vector vorticity equation model (VVM). *J. Adv. Model. Earth Syst.*, **3**, doi:10.1029/2011MS000061.

Wu, C.-M., and A. Arakawa, 2014: A Unified Representation of Deep Moist Convection in Numerical Modeling of the Atmosphere. Part II. *J. Atmos. Sci.*, **71**, 2089–2103, doi:10.1175/JAS-D-13-0382.1. http://journals.ametsoc.org/doi/abs/10.1175/JAS-D-12-0330.1.

Xiao, H., C. M. Wu, and C. R. Mechoso, 2011: Buoyancy reversal, decoupling and the transition from stratocumulus to shallow cumulus topped marine boundary layers. *Clim. Dyn.*, **37**, 971–984, doi:10.1007/s00382-010-0882-3.

Zhang, Y., B. Stevens, and M. Ghil, 2005: On the diurnal cycle and susceptibility to aerosol concentration in a stratocumulus-topped mixed layer. *Q. J. R. Meteorol. Soc.*, **131**, 1567–1583, doi:10.1256/qj.04.103. http://doi.wiley.com/10.1256/qj.04.103.

Tables
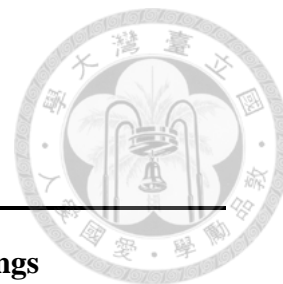
Vector Vorticity Model (VVM) environmental settings

Horizontal resolution	100 m
Vertical resolution	Below 1100m : 10 m Above 1100m : stretching to 70 m
Horizontal domain size	25.6 km × 25.6 km
Vertical domain top	about 4 km
Grid numbers	256 × 256 × 200
Time increments	1 second
Lateral boundary	Periodic
Vertical boundary	Solid wall
Vertical sponge layer	upper 30 levels
Sea Surface Temperature (SST)	291 K
Large scale divergence D_0	$10^{-6}\ s^{-1}$
Radiation scheme	Simplified scheme following Stevens[2001]

Table 1 Vector Vorticity Model (VVM) model settings. For more details upon vertical stretching grid refer to Appendix A.

Model initial profiles and conditions		
Observation data	**DYCOMS-II RF01**	**VOCALS cruise**
Inversion height	840m	1100m
Liquid Potential Temperature θ_l	289.0 K	289.5 K
Liquid Potential Temperature jump $\Delta\theta_l$	8.5 K	9.5 K
Water Vapor Mixing ratio q_v	9.0 gkg^{-1}	8.0 gkg^{-1}
Water Vapor Mixing ratio jump Δq_v	7.5 gkg^{-1}	5.5 gkg^{-1}
Cloud Water Mixing ratio jump Δq_c	0.5 gkg^{-1}	0.3 gkg^{-1}
$\kappa \equiv \dfrac{c_p \Delta\theta_e}{L\Delta q_t} = 1 + \dfrac{c_p\Delta\theta_l}{L\Delta q_t}$	0.45	0.306
Sensible heat flux	10 Wm^{-2}	7.2 Wm^{-2}
Latent heat flux	100 Wm^{-2}	30.4 Wm^{-2}
Cloud Thickness	240 m	240 m
Horizontal wind velocity	0 ms^{-1}	0 ms^{-1}
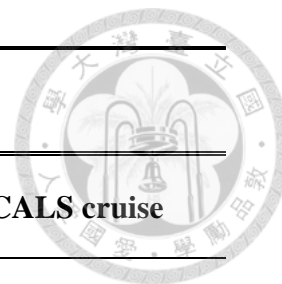
Table 2 DYCOMS-II and VOCALS initial profiles and conditions.

Figures
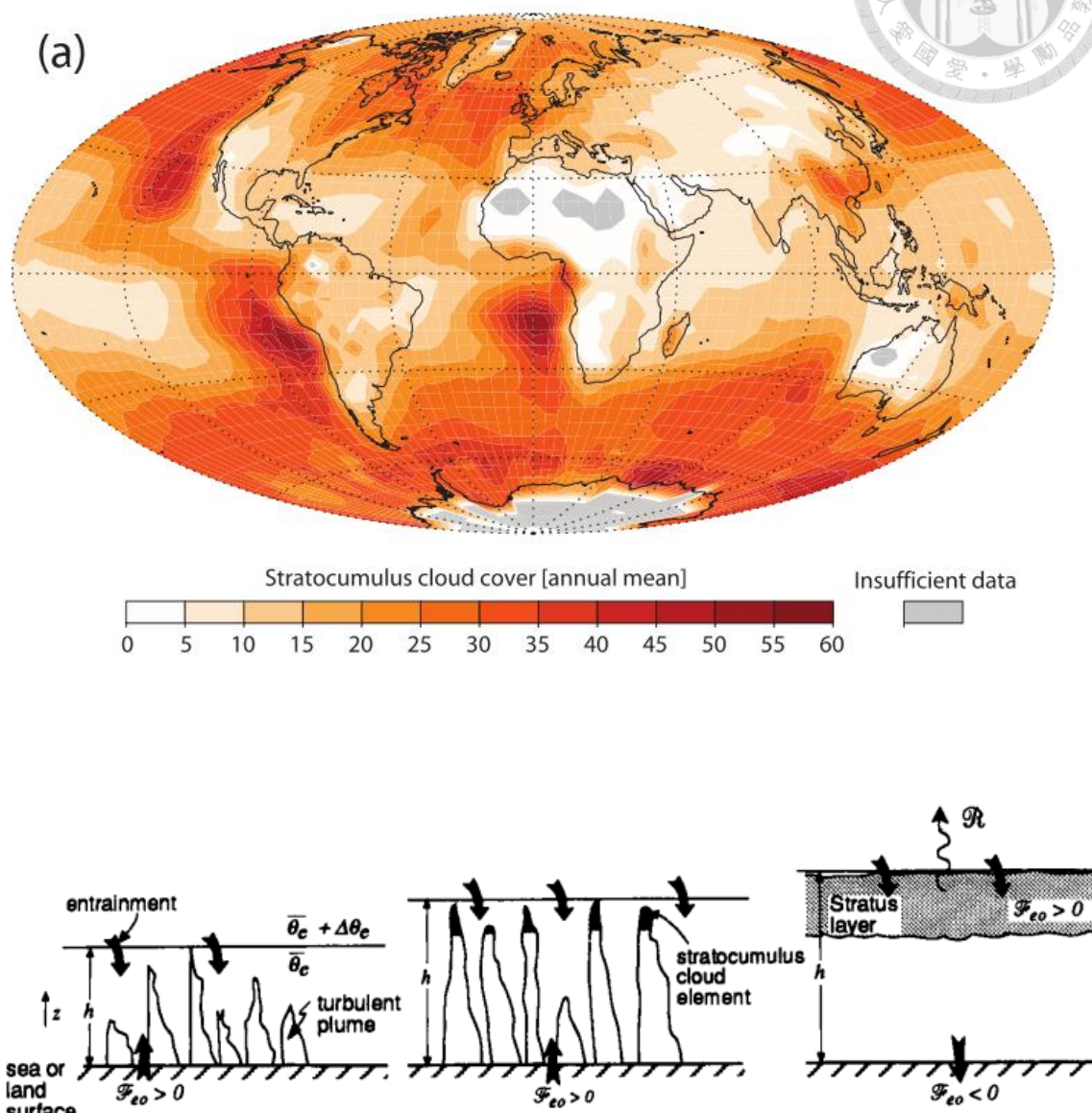
Figure.1 *Upper panel:* climatology of stratocumulus coverage. [*Credit from Wood (2012) Fig.4(a)*] *Lower panel*: conceptual model for stratocumulus forming [*Credit from Houze: Cloud dynamics]*
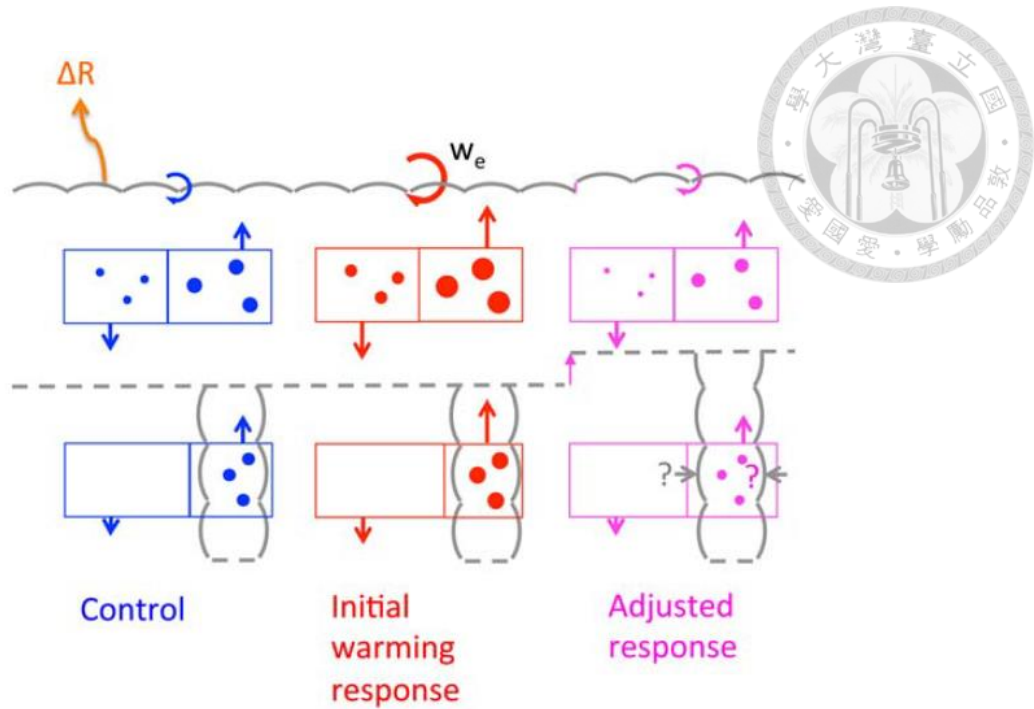
Figure.2 Diagram of how entrainment liquid-flux adjustment can lead to cloudiness reduction in stratocumulus-topped boundary layers in a warmer climate. [*Credit from Bretherton C. S., and P. N. Blossey (2014) Fig.13*]
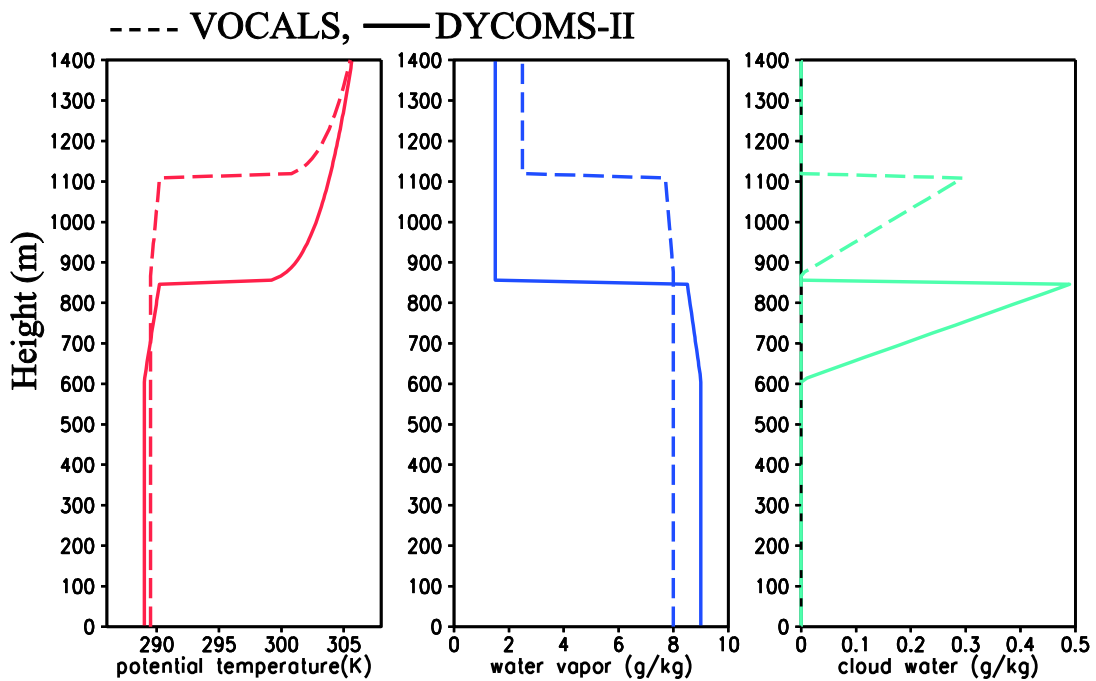
Figure.3 Initial profiles from DYCOMS-II RF01 flight and VOCALS cruise data.
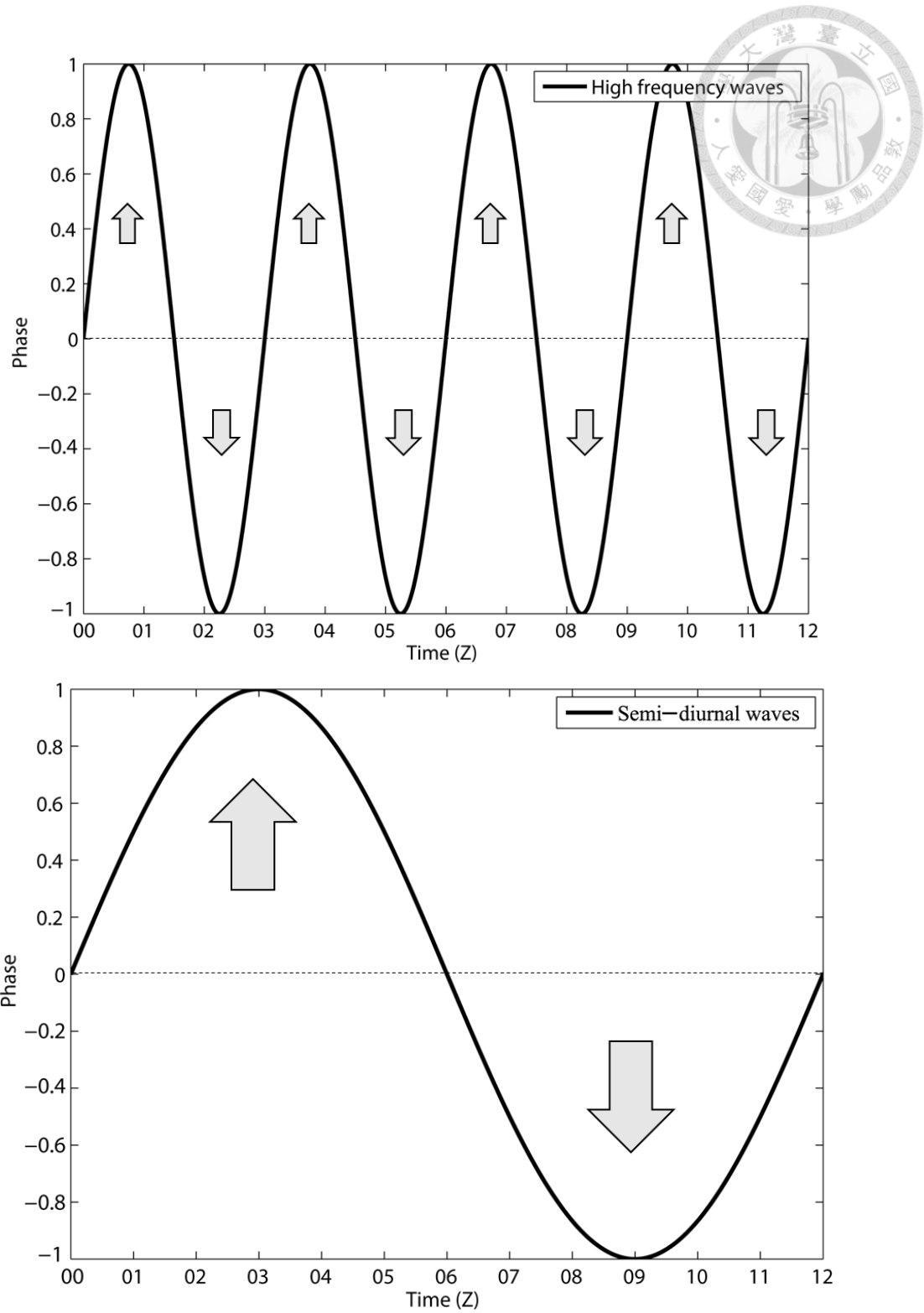
Figure.4 Mesoscale wave forcing applied to the experiment domain. High frenquency wave exhibit three hour period.
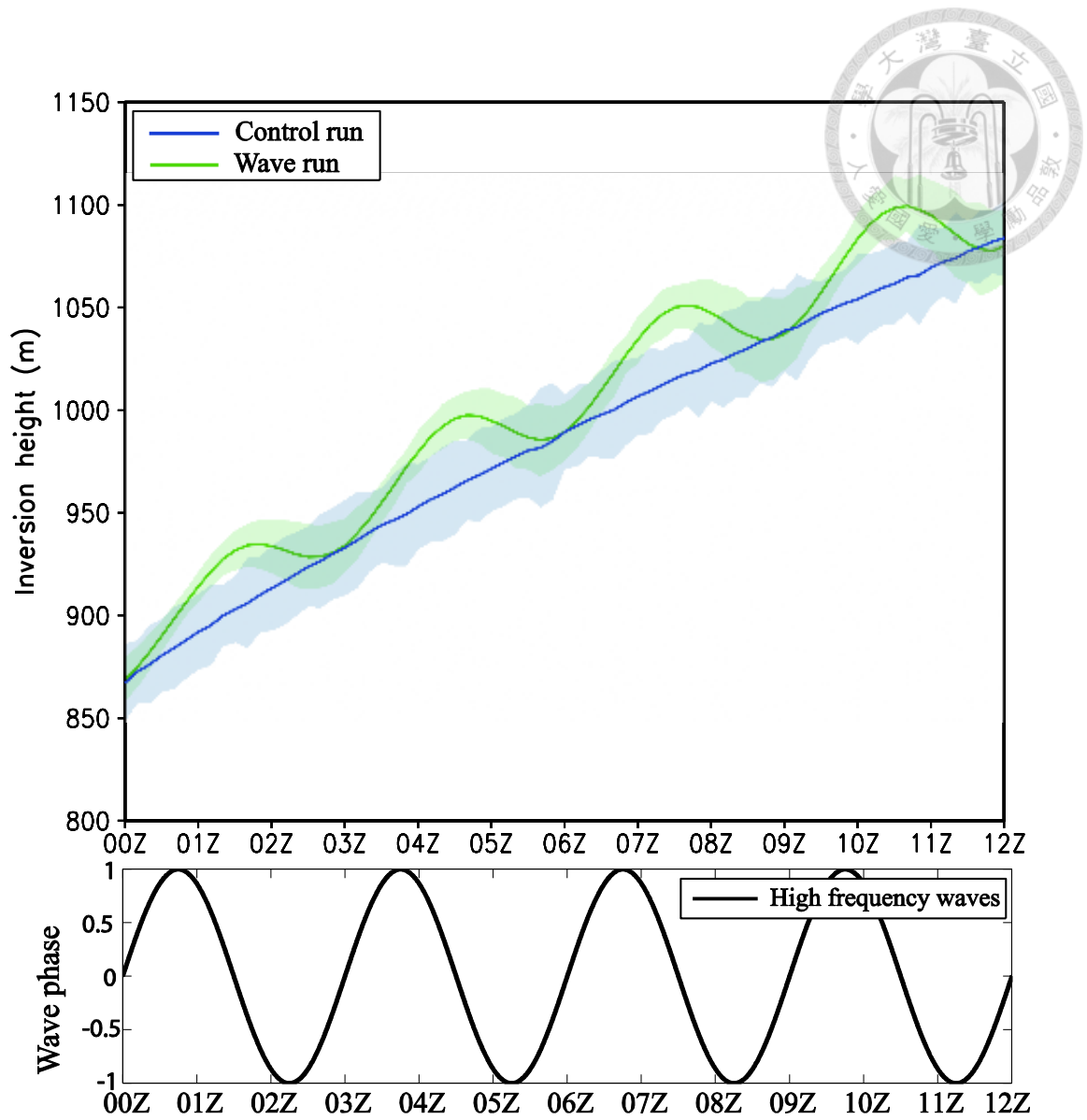
Figure. 5 Time series of domain average Inversion height, shading represent one standard deviation from mean value.
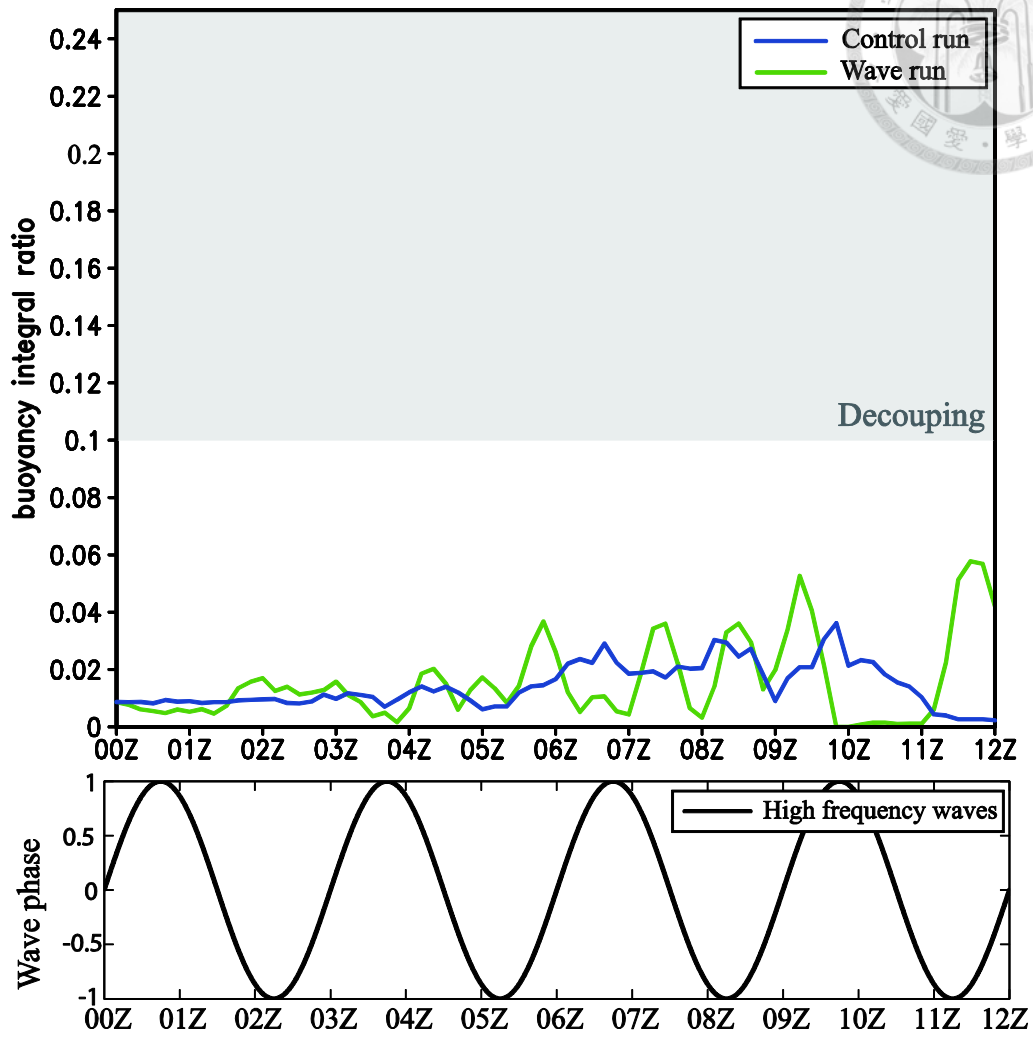
Figure.6 Time series of Buoyancy Integral Ratio (BIR), blue line represent control run, and green line represent the high frequency wave run.
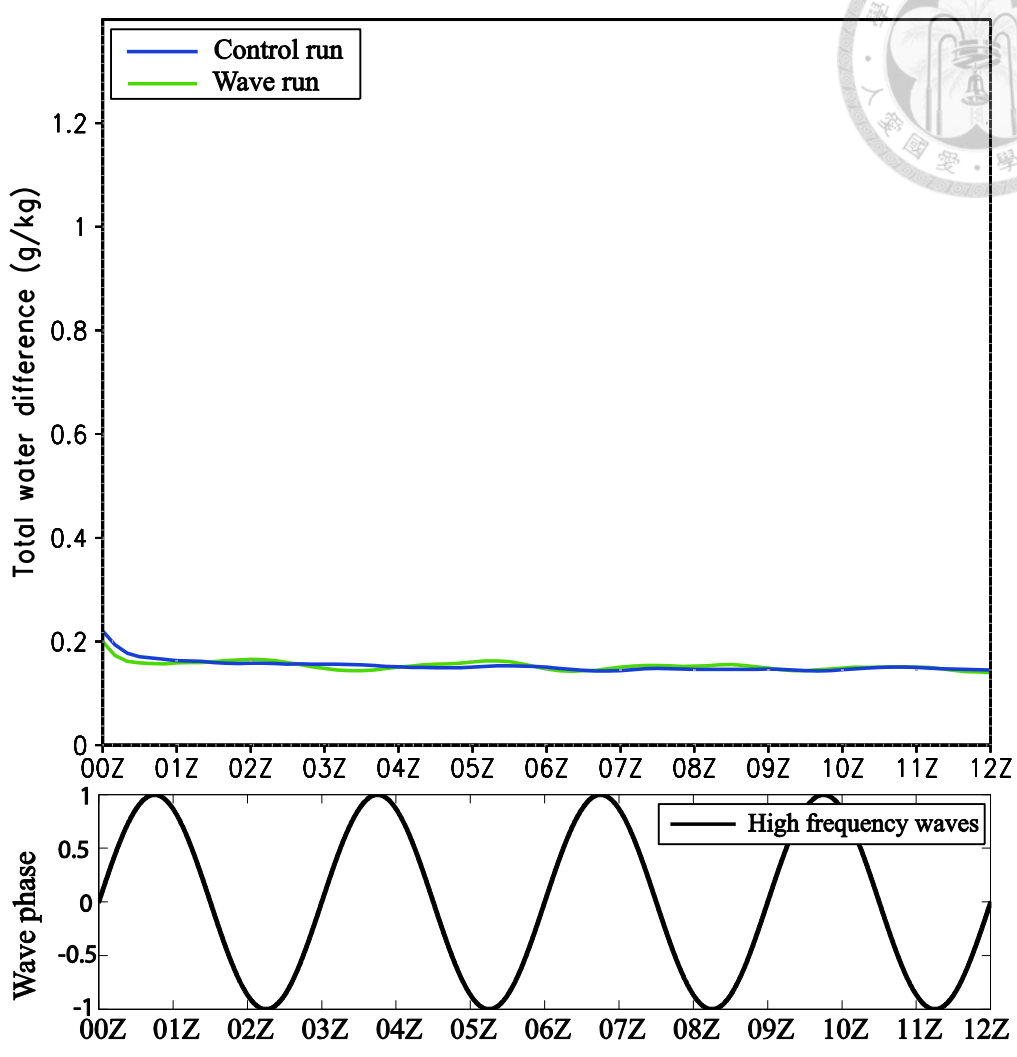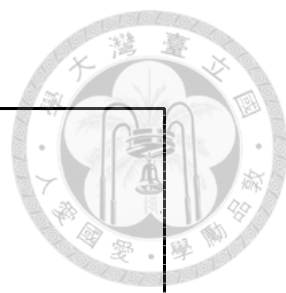
Figure.7 Time series of Total Water difference ($q_t d$), blue line represent control run, green line represent the high frequency wave run.
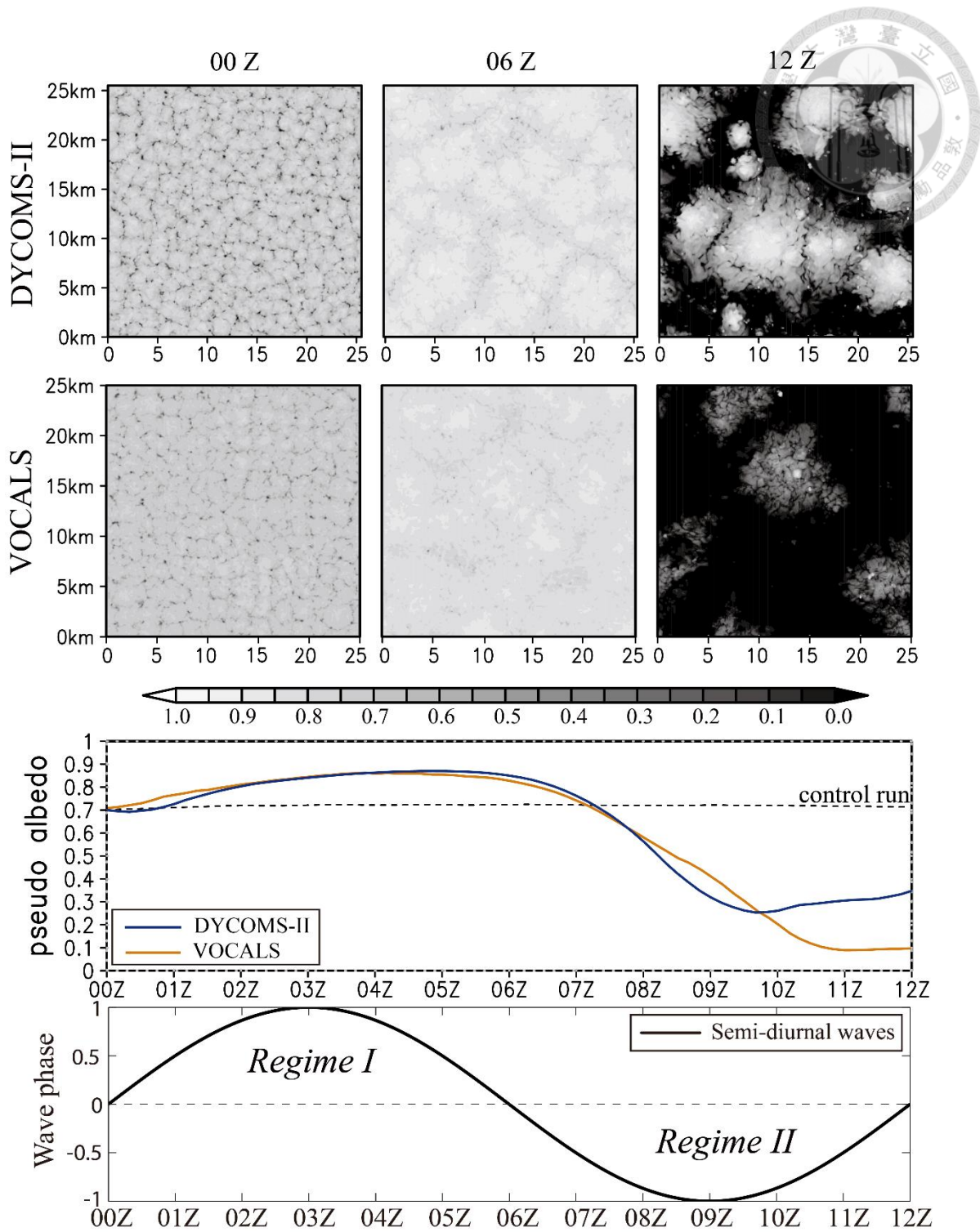
Figure.8 Pseudo albedo snapshots at 00, 06 and 12Z of control run and semi-diurnal wave run, the shading level is 0.05, sea surface albedo is about 0.10(upper panel). As for time series of domain average Pseudo albedo, blue line represents DYCOMS-II case, orange line represents VOCALS case.
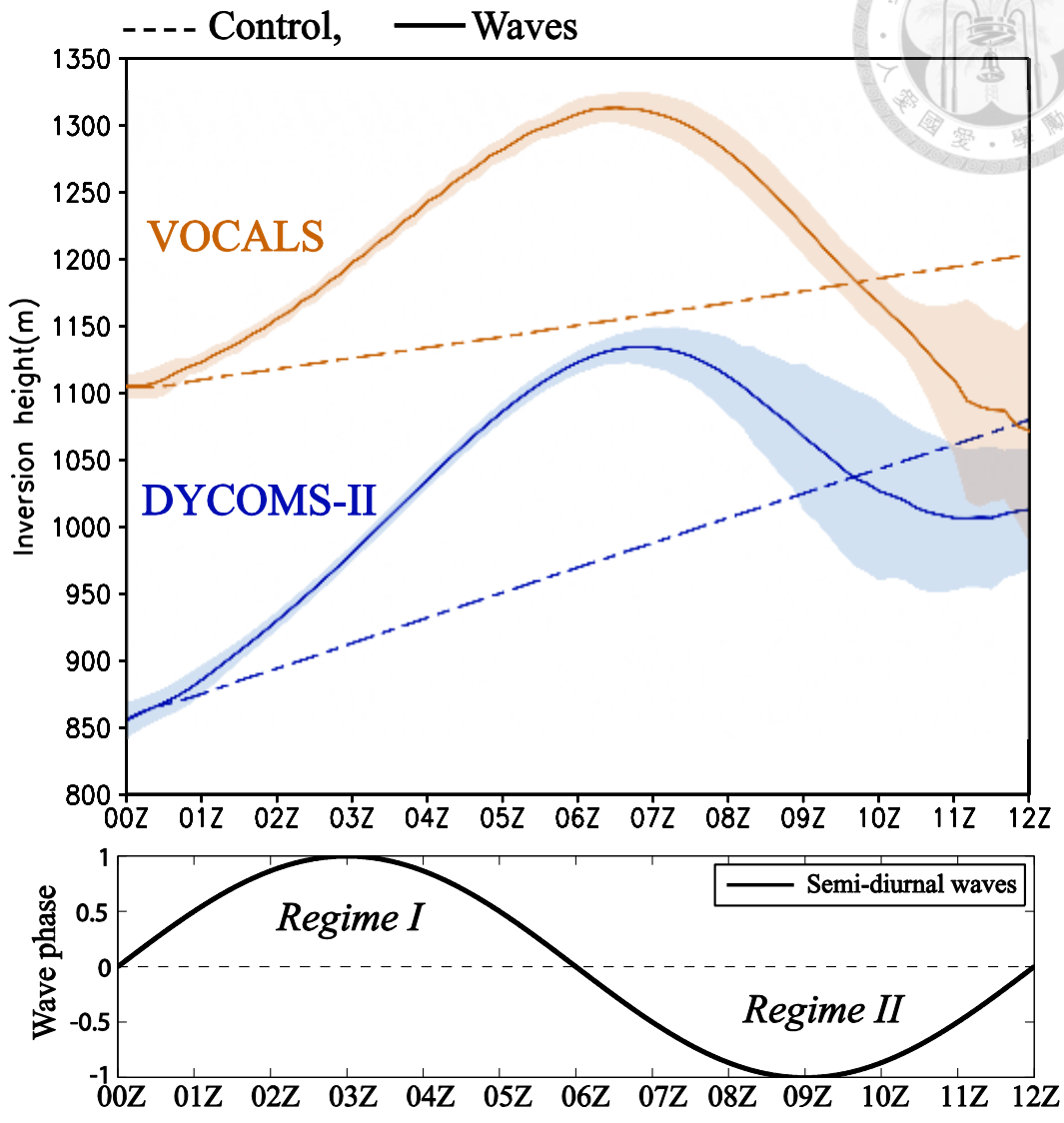
Figure.9 Time series of domain average Inversion height derived from cloud water, shading represent one standard deviation from mean value. For simplicity, only waves run shows the standard deviation.

(a) DYCOMS-II
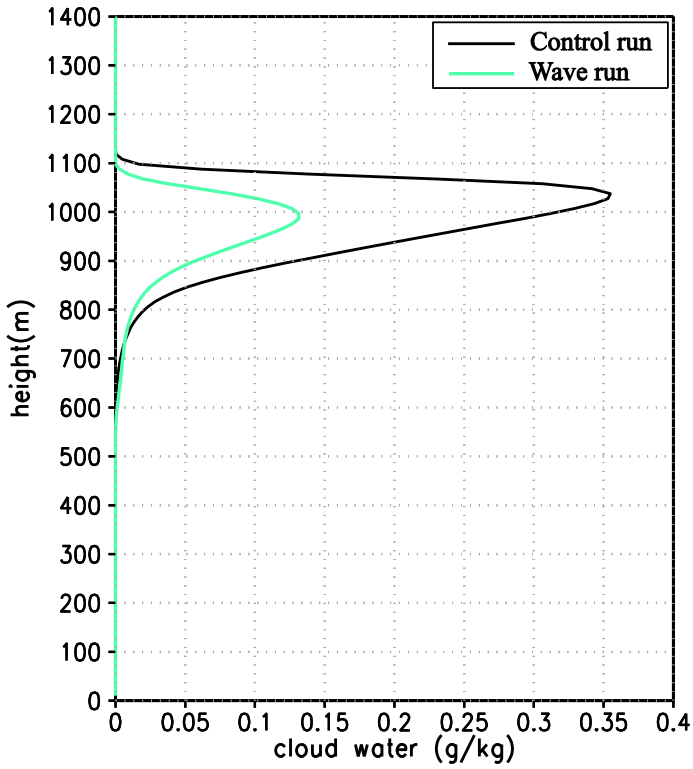
(b) VOCALS
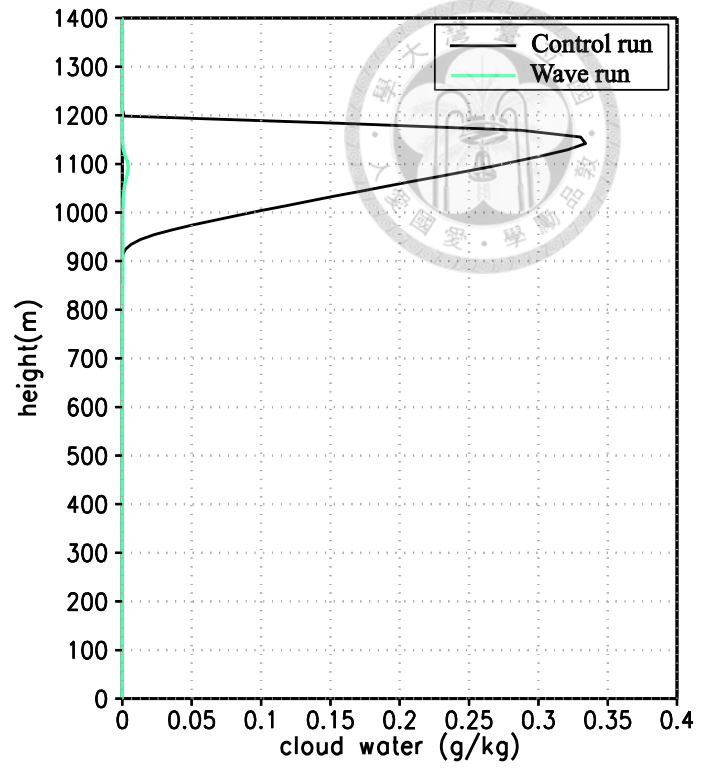
Figure.10 Vertical profiles of cloud water mixing ratio at the last experiment hour, blue line is the upsidence wave run, black line is control run.

(a) DYCOMS-II
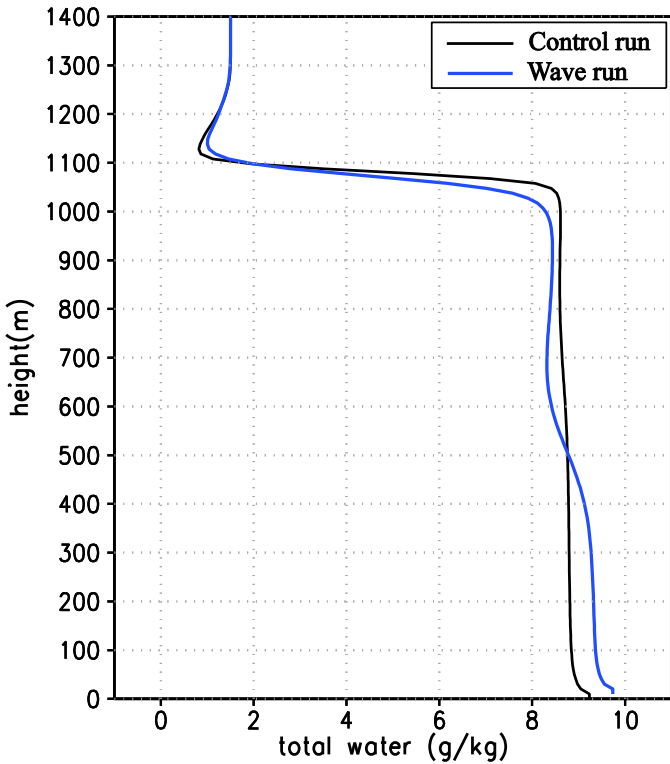
(b) VOCALS
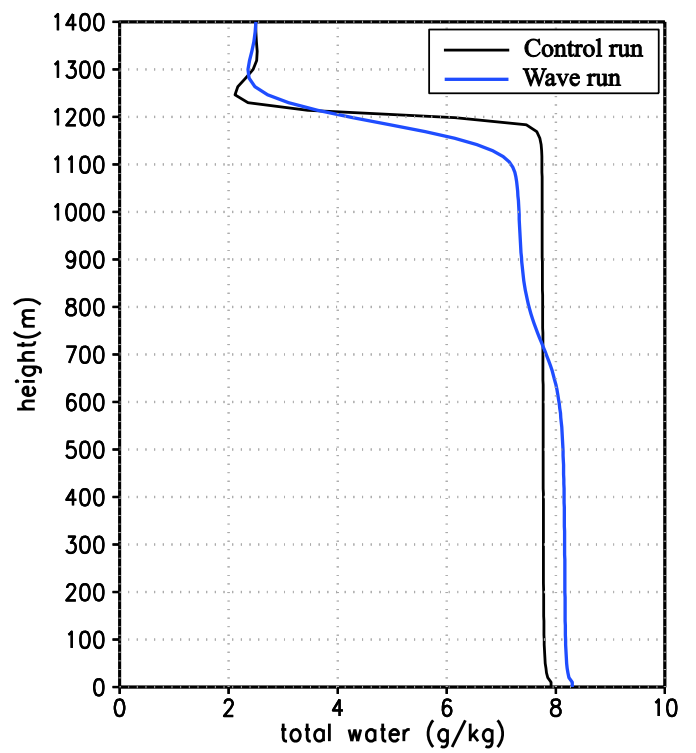
Figure.11 Vertical profiles of Total Water mixing ratio $q_t = q_c + q_v$, at the last experiment hour, blue line is the upsidence wave run, black line is control run.

60
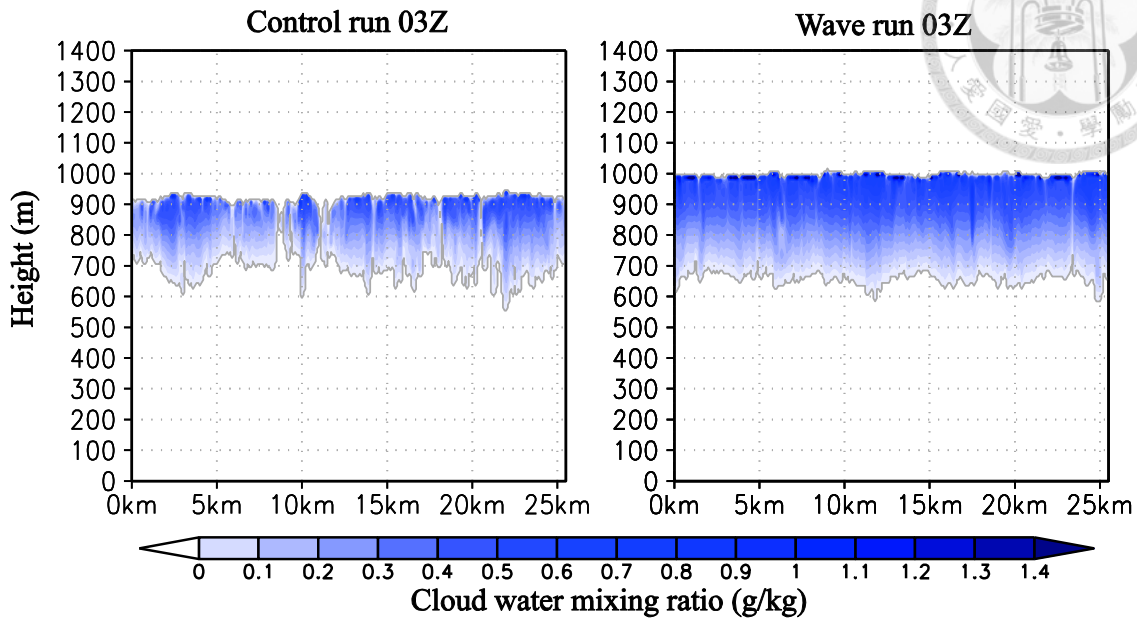
DYCOMS-II

Figure.12 Vertical slice of Cloud Water mixing ratio at the 3rd experiment hour in DY-COMS-II case, shading is the cloud water mixing ratio, grey line shows the cloud boundary.
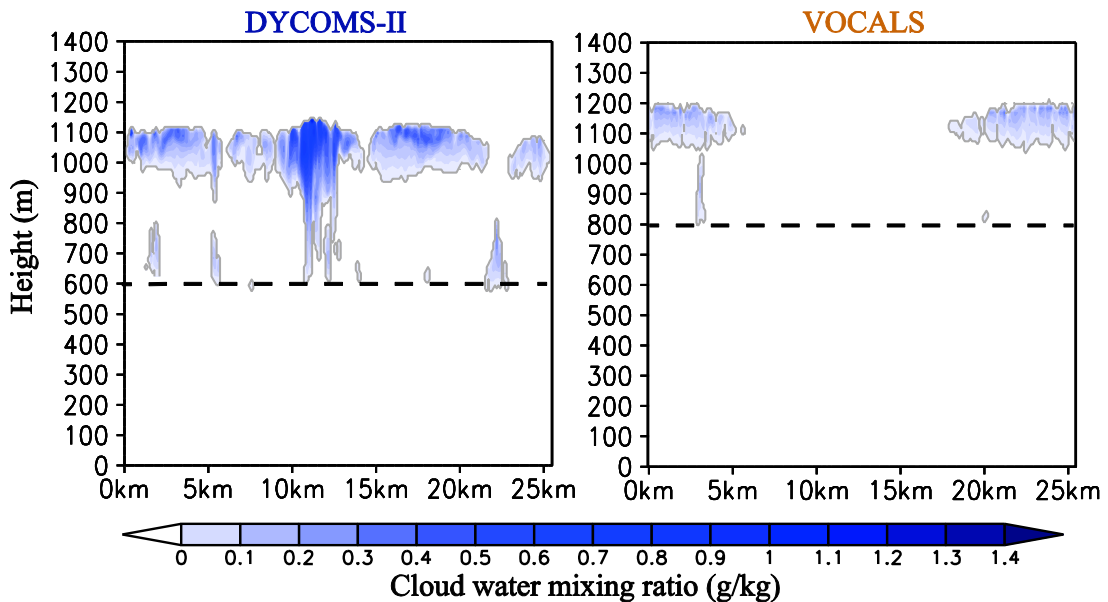
Figure.13 Vertical slice of Cloud Water mixing ratio at 09Z, shading is the cloud water mixing ratio, grey line shows the cloud boundary and black dash line represent the observed newly formed cloud layer
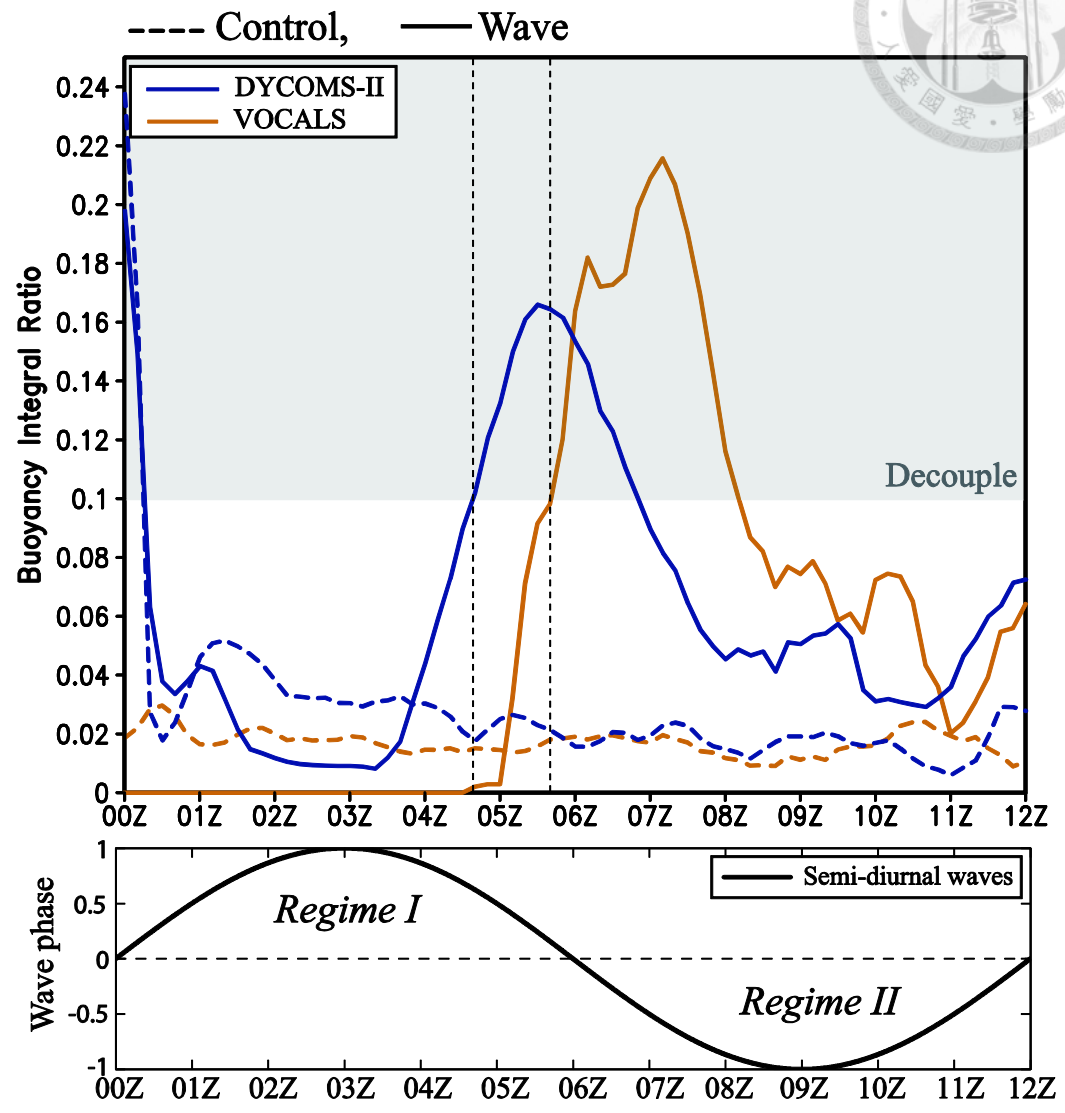
Figure.14 Time series of buoyancy integral ratio (BIR), shading represent the decoupling criterion following (Stevens2000), STBL exhibiting significant decoupling when BIR > 0.1.
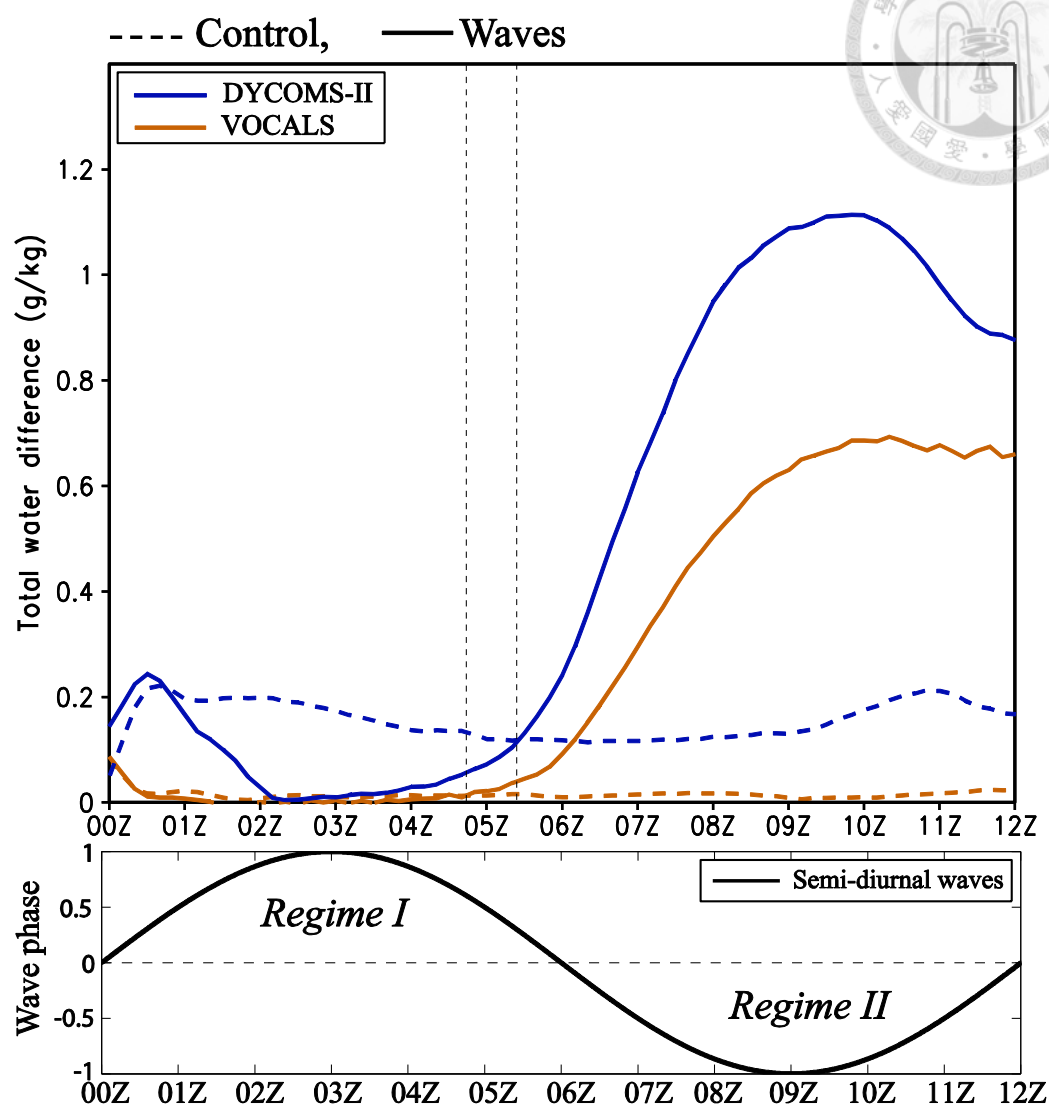
Figure.15 Time series of Total Water difference ($q_t d$), blue line is the DYCOMS-II simulation, orange line represents the VOCALS simulation.
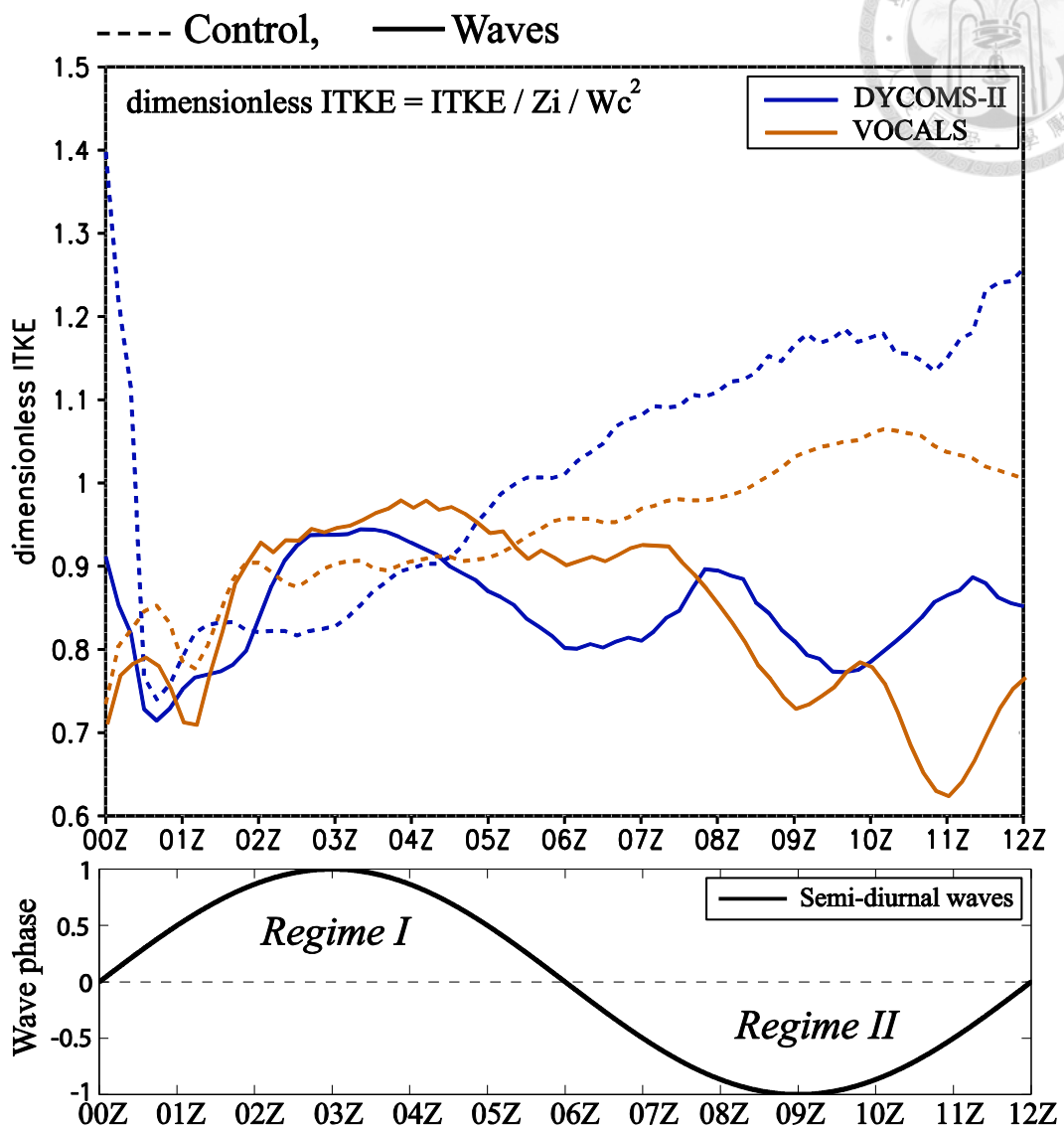
Figure.16 Time series of velocity scales and dimensionless vertical integrated TKE, blue line is the DYCOMS-II simulation, orange line represents the VOCALS simulation.
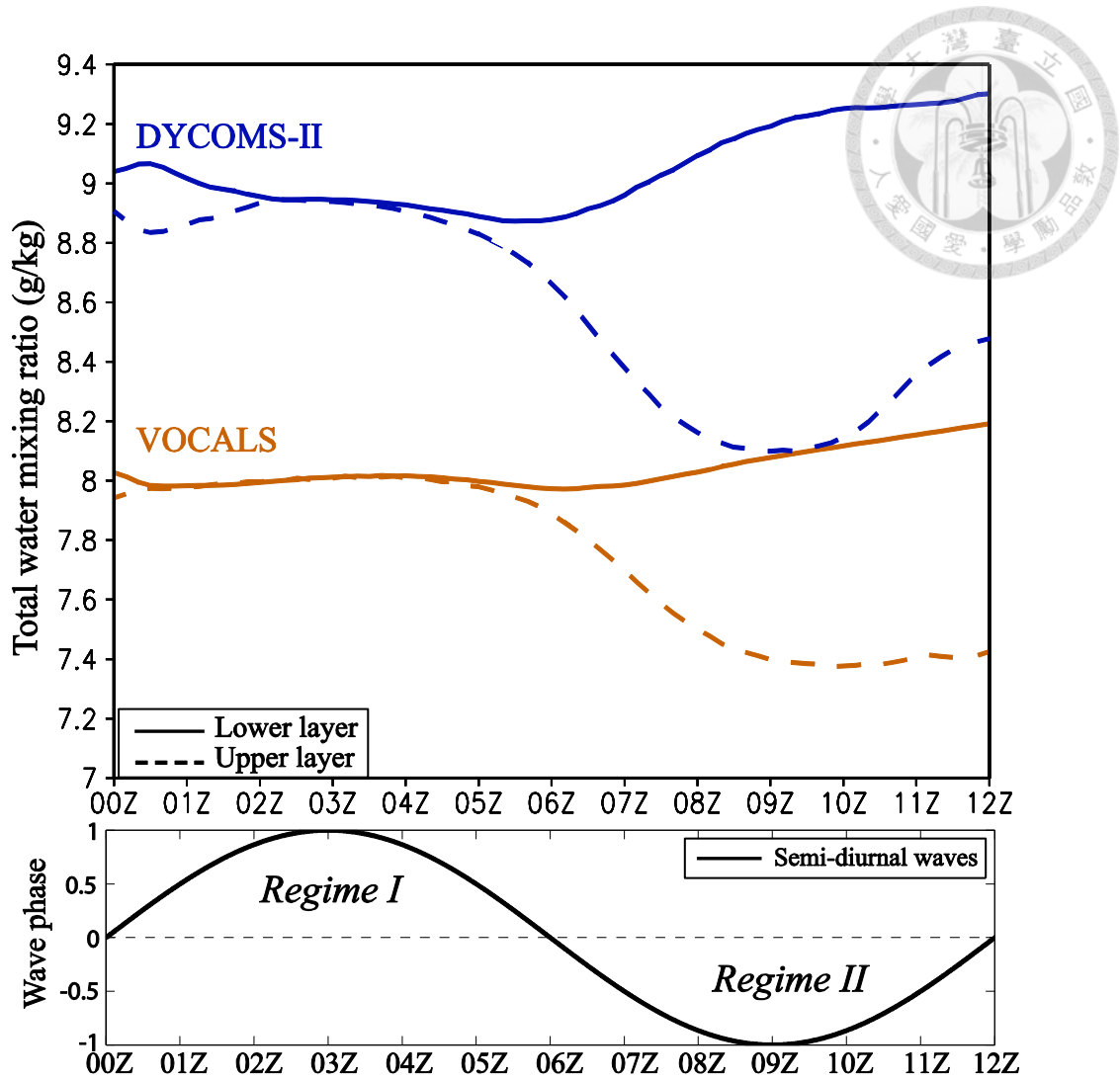
Figure.17 Time series of upper level ($0.75\ z_i$) and lower level ($0.25z_i$) Total Water mixing ratio, blue line is the DYCOMS-II simulation, orange line represents the VO-CALS simulation. Dash line is the Upper level, solid line is the lower level.
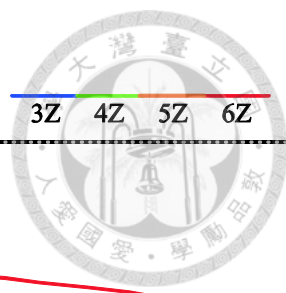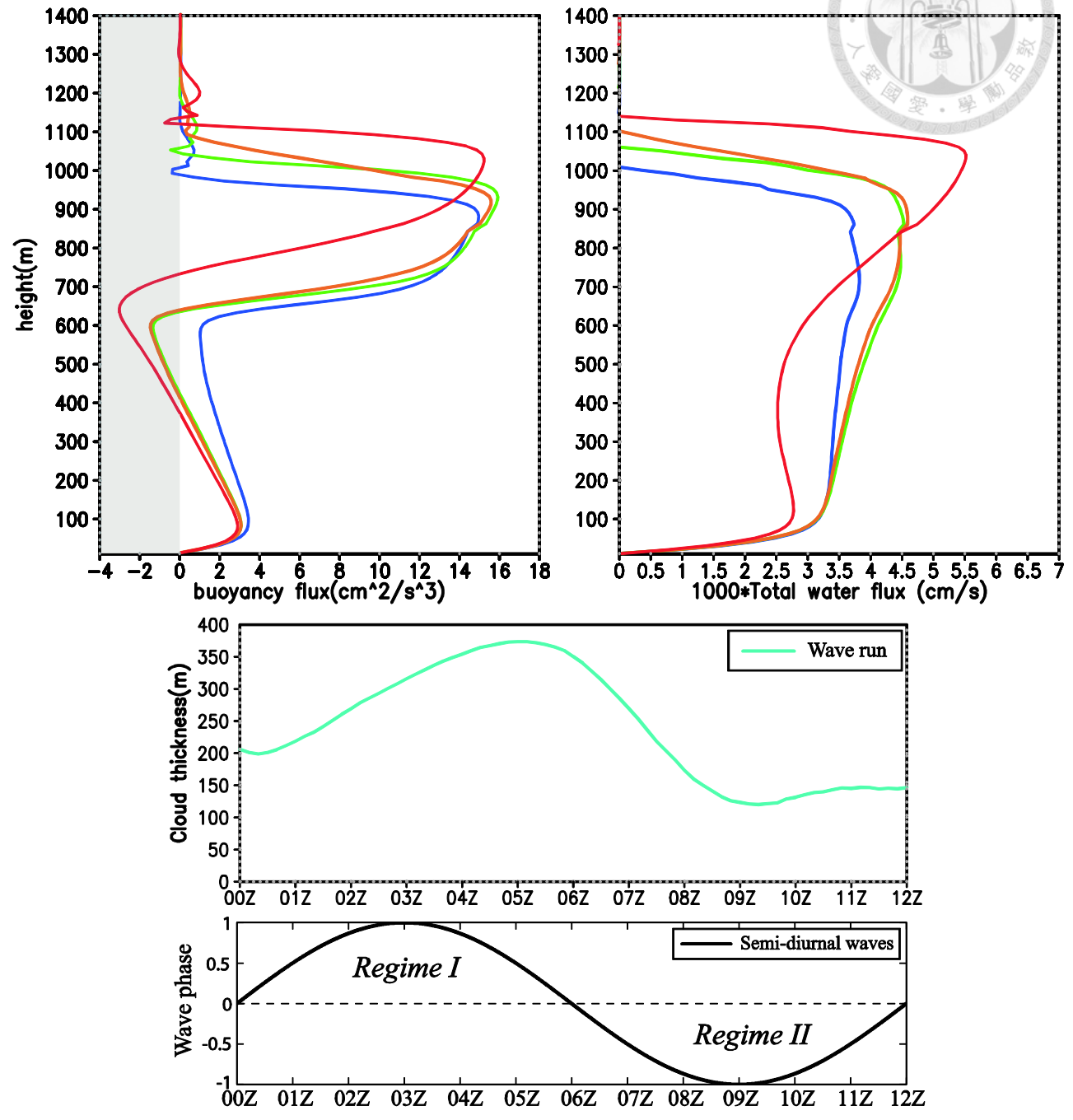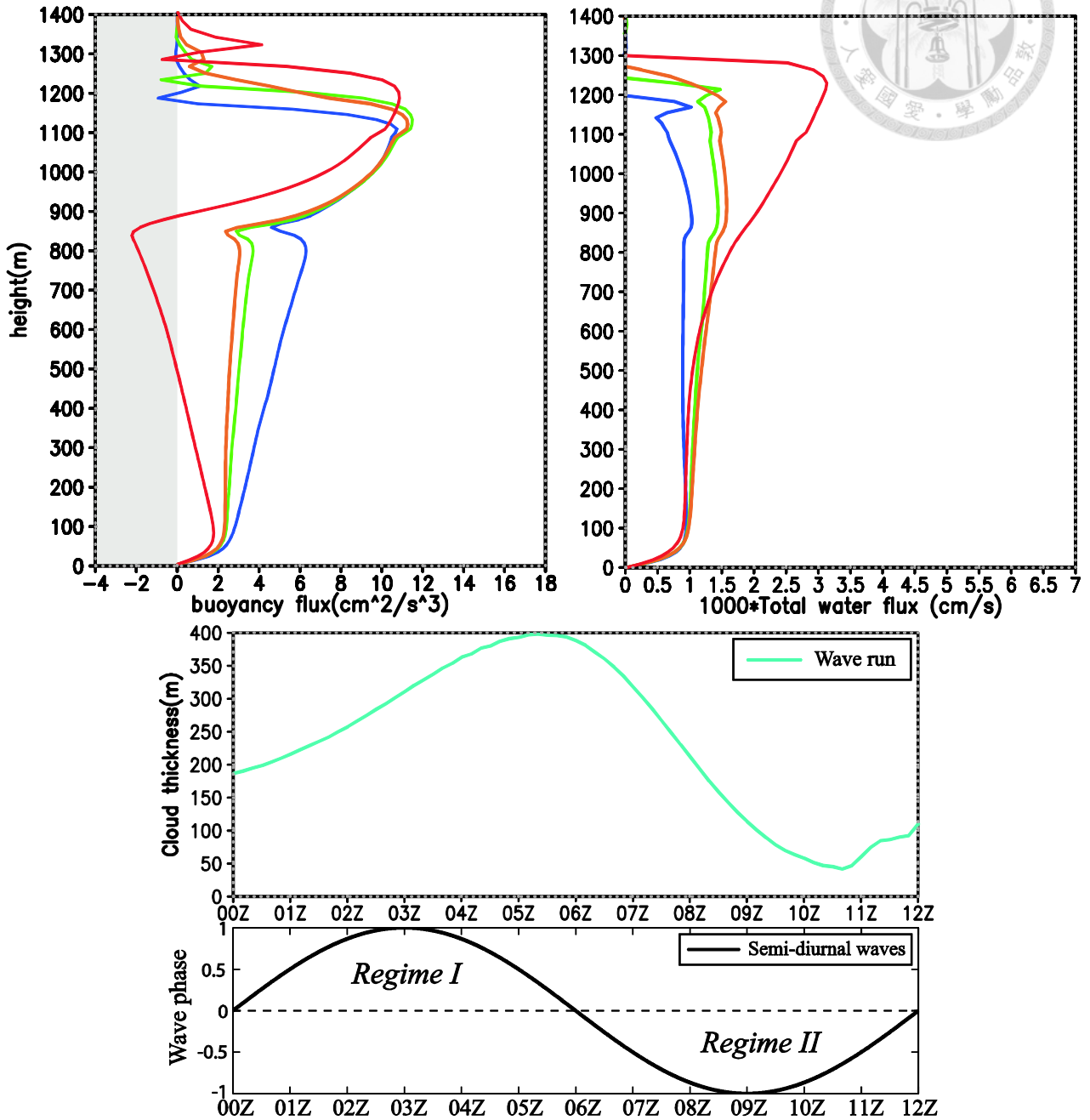
Figure.18a *Upper-left panel*: vertical profiles of buoyancy flux $w'b'$ at 03 Z to 06 Z, shading represent the negative area of $w'b'$. *Upper-right panel*: profiles of vertical Total Water mixing ratio flux $w'q_t'$ at 03 Z to 06 Z. Color bar represents the corresponding times. *Lower panel*: time series of cloud thickness derived from cloud top height minus cloud base height, colored labels indicate the same time, showing in the color bar.

Figure.18b *Upper-left panel*: vertical profiles of buoyancy flux $w'b'$ at 03 Z to 06 Z, shading represent the negative area of $w'b'$. *Upper-right panel*: profiles of vertical Total Water mixing ratio flux $w'q'_t$ at 03 Z to 06 Z. Color bar represents the corresponding times.*Lower panel*: time series of cloud thickness derived from cloud top height minus cloud base height, colored labels indicate the same time, showing in the color bar.
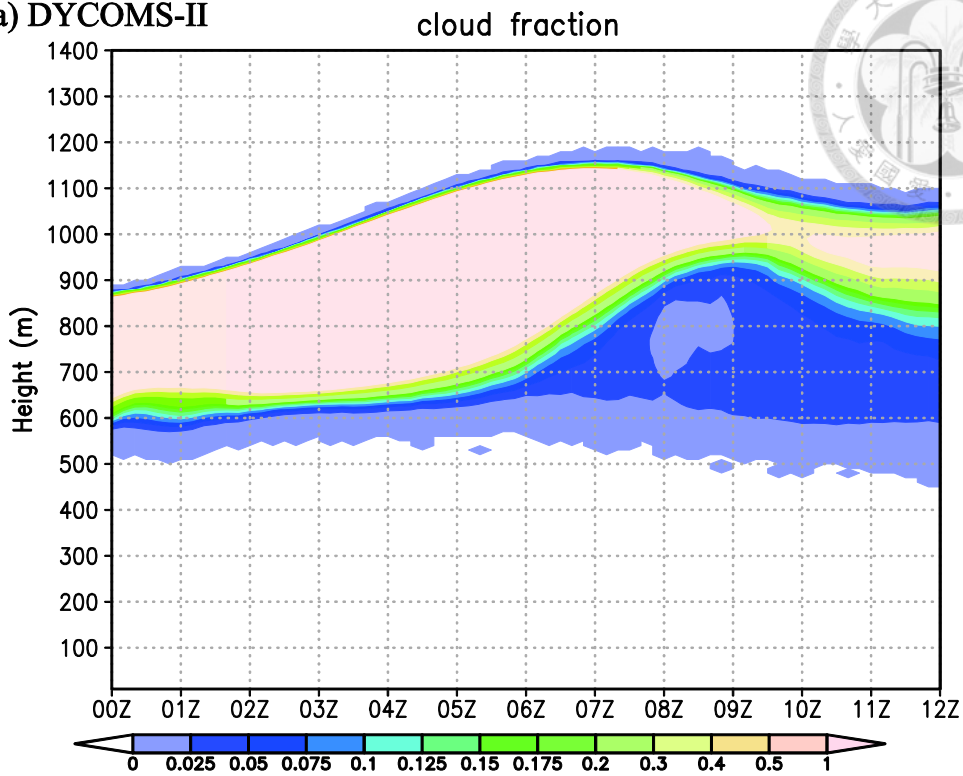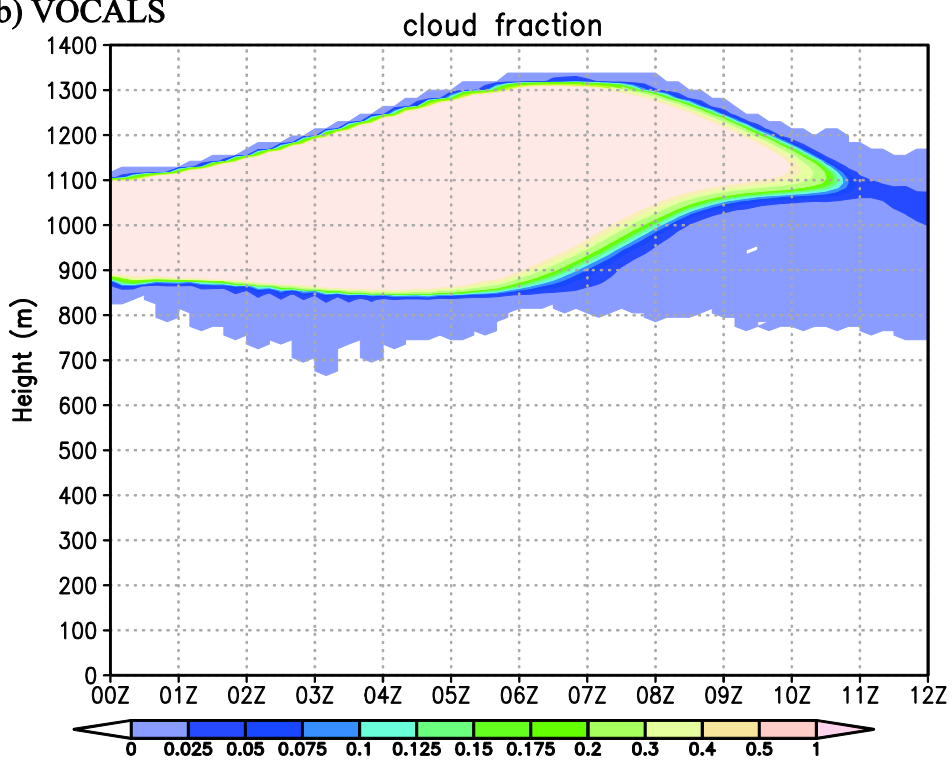
Figure.19 Cloud fraction in DYCOMS-II and VOCALS simulations. For clarity, the color scale is amplified in lower cloud fraction value and above 0.5 is all set to orange and Red.
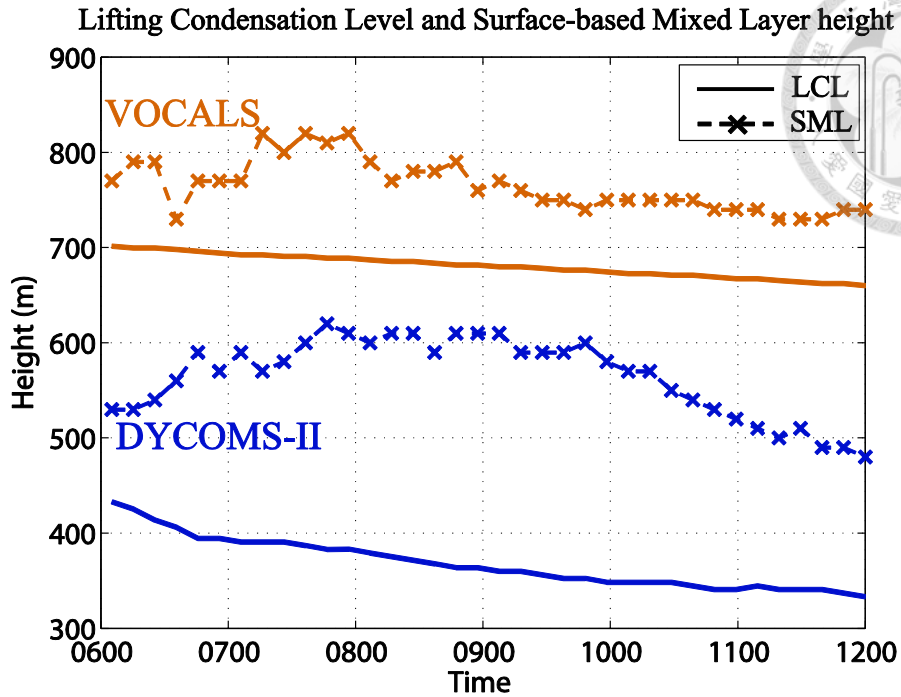
Figure.20 Lifting Condensation Level (LCL) and Surface-based Mixed Layer height computed from maximum gradient height of total water in two simulations. Only the last six hours are plotted.
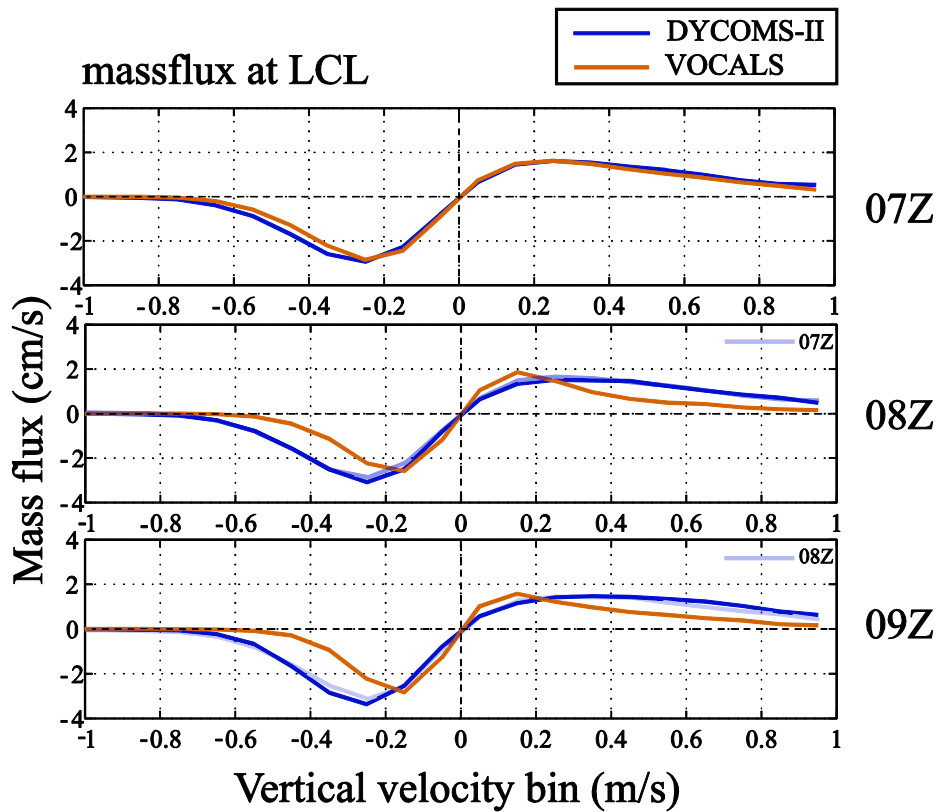

Figure.21 Mass flux at LCL in two simulations at 07~09 Z, note that the transparent blue line represent the DYCOMS-II mass flux at the last hour.

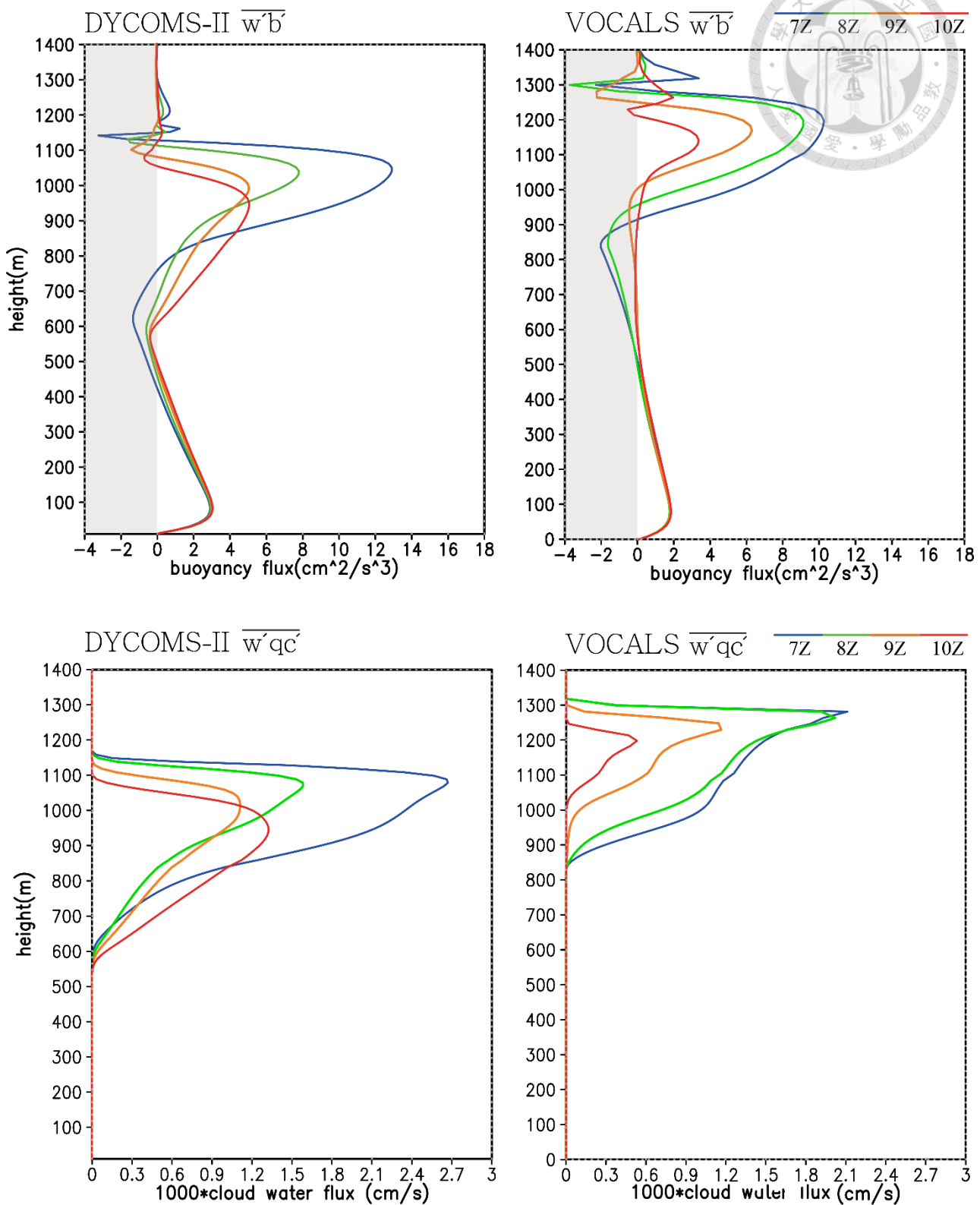**Figure.22** *Upper panel:* buoyancy flux at 07~10 Z in two wave run simulations, shading area represent the negative value of buoyancy flux. *Lower panel:* vertical cloud water flux at 07~10 Z in two wave run simulations.

Appendix A   Inversion height hysteresis

Presumably, under periodic forcing the inversion height should back to original height, but from result it seems STBL exhibit hysteresis, why?

This study introduce Mixed-Layer Model to help us answer this question by compare the result with VVM result. We simply use VVM output cloud water derived Liquid Water Path and feed them into MLM:

$$\frac{\mathrm{d}h}{\mathrm{d}t} = W_E - Dh \tag{A}$$

$$h\frac{\mathrm{d}S_l}{\mathrm{d}t} = -\frac{\partial}{\partial z}\left(\overline{w'S_l'}\right) = C_T V(S_{lo} - S_l) + W_E(S_l^+ - S_l) - \frac{\Delta F_R}{\rho} \tag{B}$$

$$h\frac{dq_t}{dt} = -\frac{\partial}{\partial z}\left(\overline{w'q_t'}\right) = C_T V(q_{to} - q_t) + W_E(q_t^+ - q_t) \tag{C}$$

$$\alpha = W_E \frac{\Delta S_l}{\Delta F_R/\rho} \tag{D}$$

The entrainment velocity W_E is determined by radiative divergence F_R, furthermore, the radiative divergence ΔF_R in derived from Liquid Water Path. By feeding LWP into MLM we can derive ΔF_R and thus entrainment velocity W_E. In addition to calculate the S_{lo} and q_{to} needed to acquire the same surface fluxes in VVM to compare the result with, we also tune the entrainment efficiency α in eq.(D) to fit the result using VVM so that at the end of the experiment the inversion height remain the same in control run. In here we only care about the height at the end of the experiment so

we neglect the evolution of the inversion height. By conducting this, we can see how the

two layer structure affect the PBL height development. Since ΔF_R is relative to LWP and

in turn W_E, what we have done by putting VVM output LWP in MLM means that in MLM

all LWP are contribute to the strength of ΔF_R and W_E, namely, LWP represent the entire

cloud decks in MLM; In contrast, in VVM the cloud layer may exhibit separation, for

entrainment at inversion, only upper part cloud layer contribute to the entrainment

strength. In the last, the VVM and MLM inversion height difference then stands for the

effect of STBL decoupling.

The result reveals that in the MLM result it even exhibit higher inversion height in

the last, and VVM result shows lower height compare to control run. The higher inversion

may partly attribute to the non-linearity of the Mixed-Layer Model equations. From

eq.(A), under the wave forcing it become:

$$\frac{\mathrm{d}h}{\mathrm{dt}} = W_E - (D_0 + D_m)h \qquad (E)$$

Where, D_m is the wave induced divergence, D_0 is the large scale divergence.

Physically we can realized that when wave cause inversion height changes, at the new

level, the wave and large scale subsidence induced height changes may differ from the

beginning, which is reflected in the above equation. Also, at higher levels below 3km the

upsidence wave strength is stronger, stated in (Garreaud and Munoz 2004).
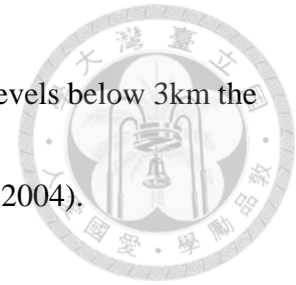
Even though the non-linearity illustrate the disparity of MLM result at the end of

experiment, the VVM predicted inversion height even exhibit lower than MLM, which

represents the decoupling impact on the STBL. The hysteresis is owing to the non-linear-

ity of the STBL. Besides the non-linear nature, the STBL decoupling serves as the major

origin of such inversion height hysteresis.
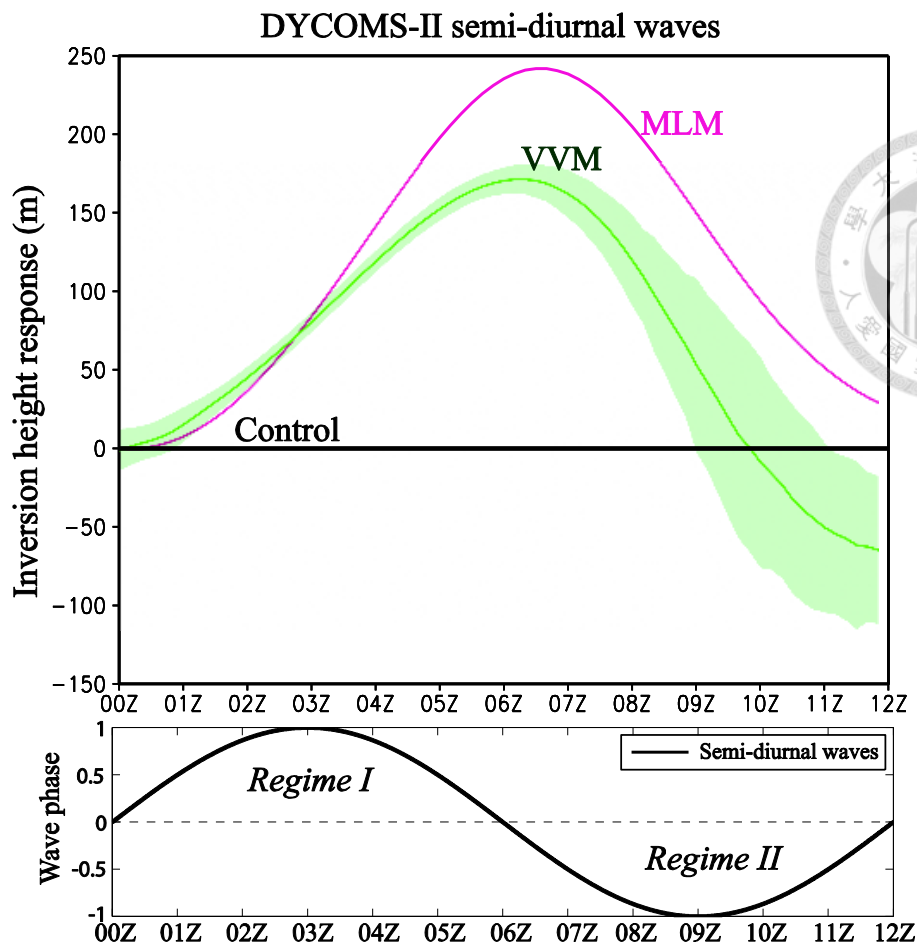
Mixed Layer Model (MLM) environmental settings

Time increments	1 second
Time integration scheme	Runge-Kutta fourth order
Drag coefficient C_T	0.001
Wind velocity for flux calculation	10 ms^{-1}
Entrainment efficiency α	0.7
Large scale divergence D_0	$10^{-6}\ s^{-1}$
Radiation scheme	Simplified scheme following Stevens[2001]

Table A   Mixed Layer Model (MLM) model settings.

Appendix B   Mass flux analysis
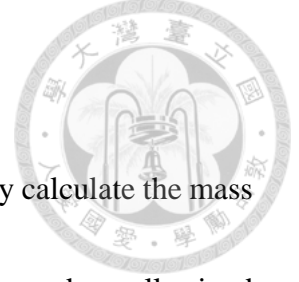
To realize how STBL evolve over time at certain levels, this study calculate the mass flux following (Ghate et al. 2014), which analyze the STBL evolution under well-mixed state and decoupled state from VOCALS sounding data. Cumulus parameterizations consider the updraft mass flux as a diagnostic variable, and the mass flux can thus be derived from data using the plume decomposition technique proposed by (Arakawa and Schubert 1974), which is:

$$M = \sum_i \sigma_i \times (w_i - \bar{w}) \tag{F}$$

In which, M is the computed mass flux, w_i is the binned vertical velocity, $\bar{w}$ is the domain average of vertical velocity (Ghate use hourly mean vertical velocity to adapt to the sounding data), and σ_i is the fraction of certain strength of vertical velocity in the domain. Mass flux was calculated for each $0.1 \text{ m} s^{-1}$ velocity bin from $-3 \text{ m} s^{-1}$ to $3 \text{ m} s^{-1}$. It can be interpreted as turbulent mass flux contribute to Total turbulent mass flux by certain bins of velocities.

To investigate the time evolution of mass flux at certain levels, we conduct Hovmoller diagram of turbulent mass flux, furthermore, plot the zero value line to help us identify the strength variation of turbulent mass flux over the time.
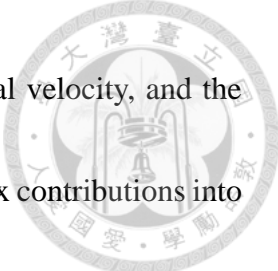
Fig.B(upper panel) represents the turbulent mass flux time evolution at the middle of STBL in control run and wave run. We observe that in control run, DYCOMS-II simulation the turbulence exhibit larger intensity than VOCALS simulation, seen from the contour line, which represents the zero value of mass flux at certain velocity bins. Furthermore, in wave run, it shows significant wave pattern in first six hours, larger increase of mass flux is observed within the ∓ 1.5 ms^{-1} bins; at the last six hours, STBL decoupled and cloud dissipated so that the turbulence strength and thus mass flux decreased greatly. However, we also observe that in the last six hours the updraft turbulent mass flux still exhibit some strength than downdraft turbulent mass flux shown in the yellow shading of updraft and the zero contour line. Such response is attribute to the newly formed stable layer after STBL decoupled. At this level, we can see the cumuliform cloud formed shown in Fig.15a, 15b, which correspond to the larger value of updraft turbulent mass flux.

Fig.B(lower panel) illustrates the mass flux evolution near the cloud base, the key features of mass flux in subcloud level is that the tail of the distribution of the downdraft mass flux is longer than that of the updraft mass flux at all levels; yet the updraft features smaller distribution but stronger mass flux contribution in low velocity bins, which reflect the circulation pattern of smaller region of downdraft and broad region of updraft. The

turbulent mass flux contributions are not symmetrical to zero vertical velocity, and the

most substantial asymmetry is the confinement of the updraft mass flux contributions into

a more narrow range of vertical velocity bin. Similarly, the turbulent mass flux also shows

significant wave pattern in first six hours, but exhibit larger downdraft above the -

$1.0 \text{ m}s^{-1}$ bins, and smaller updraft mass flux peaks. As for the last six hours, different

from $z/z_i = 0.5$ result, both simulations did not show the significant updraft mass flux,

especially in VOCALS run, the mass flux contribution are both at lower velocity bins

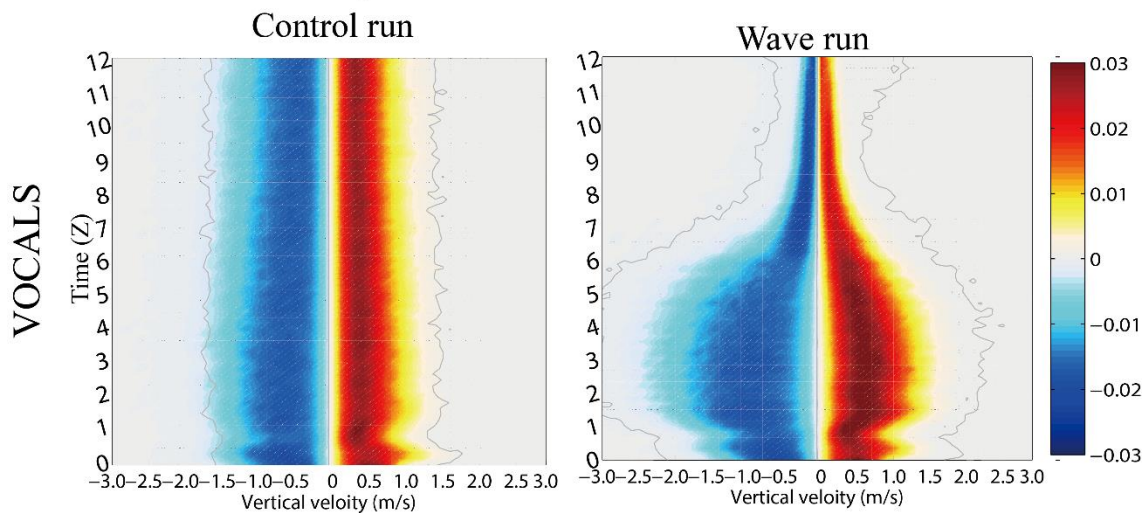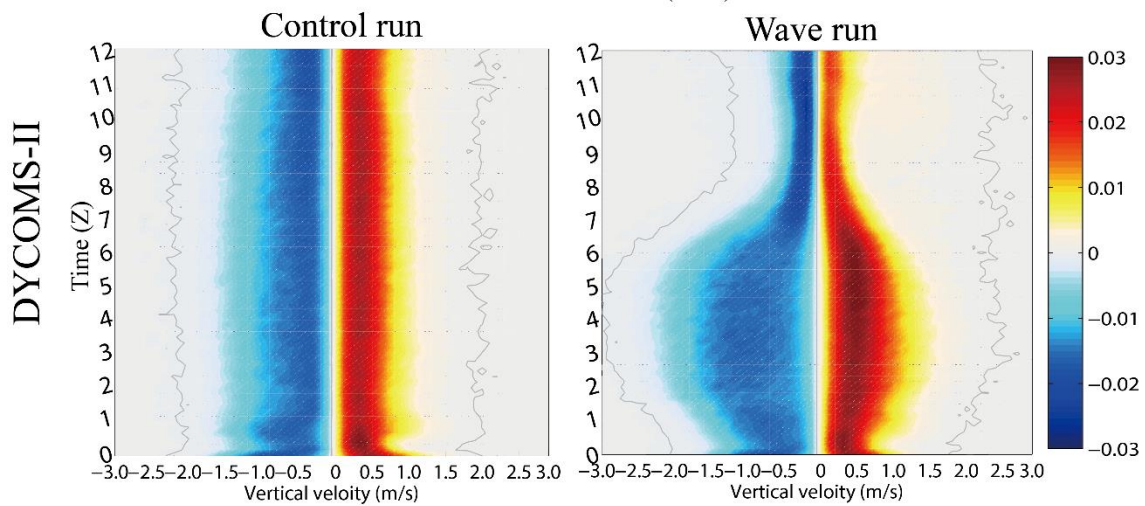owing to the cloud deck cleaning by the semi-diurnal waves.
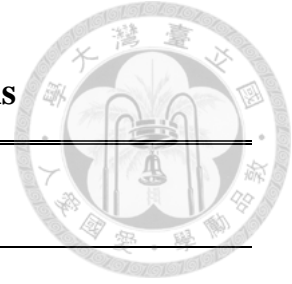
z/zi=0.5

Turbulent mass flux (m/s) at z/zi=0.5
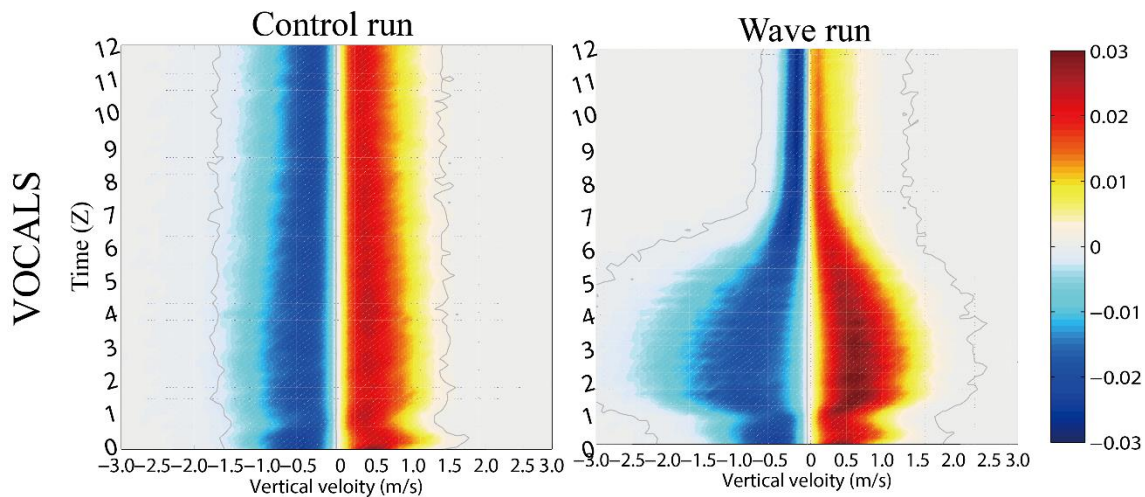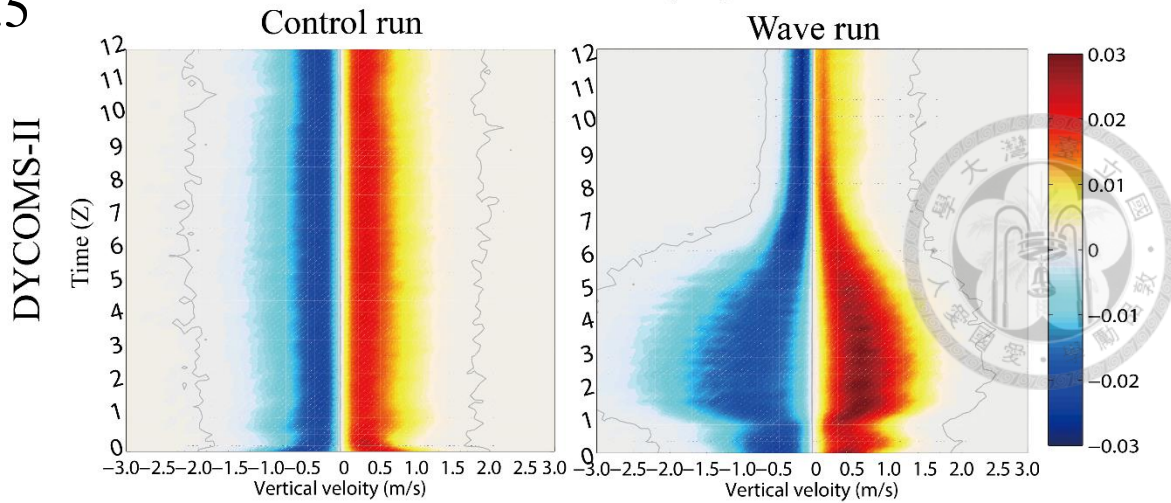
z/zi=0.7

Turbulent mass flux (m/s) at z/zi=0.7

Appendix C   Abreviations and notations

Acronym

Symbol	Denotes
STBL	Stratocumulus-Topped Boundary Layer
PBL	Plantary Boundary Layer
SML	Surface-based Mixed Layer
VVM	Vector Vorticity Model
MLM	Mixed-Layer Model
ELF	Entrainment-Liquid water Flux feedback
CTEI	Cloud Top Entrainment Instibility
CIFKU	Conditional Instability of the First Kind Upside-down
CIFK	Conditional Instability of the First Kind
BIR	Buoyqncy Integral Ratio
$q_t d$	Total Water mixing ratio(q_t) $d$ifference
ITKE	vertical Intergated Turbulent Kinetic Energy
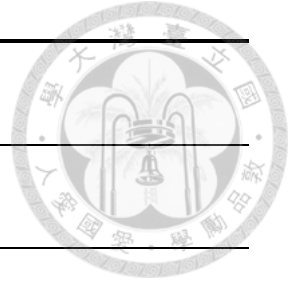
Notations

Symbol	Denotes
Z_i	Inversion height
D_0	Large scale divergence
D_m	Wave induced divergence
C_T	Drag coefficient
θ_e	Equivalent Potential Temperature
θ_l	Liquid Potential Temperature
q_c	Cloud water mixing ratio
q_t	Total water mixing ratio
$w'b'$	Vertical buoyancy flux
$w'q_t{'}$	Vertical total water flux
$w'q_c{'}$	Vertical cloud water flux

Appendix D   Vertical stretching grid

The vertically stretching grid is proposed by (Wilhelmson and Chen 1982), which mapping the actual vertical coordinate Z into Z'. A constant grid interval dZ' is used in Z' coordinate system so that the actural height Z of a grid point can be derived from the equation below:

$$Z = (C_1 + C_2 Z')Z'$$

$$Z' = \begin{cases} kdZ' \\ (k - 0.5)dZ' \end{cases} \ (stagger\ grid)$$

$$C_2 = \frac{(dZ - dZ')}{dZ(H - dZ)}$$

$$C_1 = 1.0 - C_2 H$$

In which, C_1 and C_2 are constants based on dZ', dZ and H is the domain depth. In our study, $dZ' = 10m,\ dZ = 70m$ so that $C_1 = 0.1307,\ C_2 = 1.74 \times 10^{-4}\ m^{-1}$. As for the vertical derivitive $\frac{\partial F}{\partial Z}$ of any function F, it can be transformed into Z' coordinate by chain rule:

$$\frac{\partial F}{\partial Z} = FNZ \frac{\partial F}{\partial Z'}$$

The mapping factor FNZ is defined as:

$$FNZ = \frac{1}{C_1 + 2C_2 Z'}$$

The above method is the original transformation method for vertical grid, the resolution

go higher near the surface; however, in our study, we want to keep high resolution below

and near the STBL to resolve the turbulence and its mixing process, which is the key role

in boundary layer. To achieve this, we modified the transform equation and mapping

factor, preserve higher solution below certain level kT. Below kT_{th} level, FNZ is set to

$\frac{dZ'}{dZ}$ and $Z = Z'$; at $kT + 1_{th}$ level, FNZ is set to $\frac{dZ'}{Z(kT+1)-Z(kT)}$. Figure below showing

the result vertical spacing used in our study.
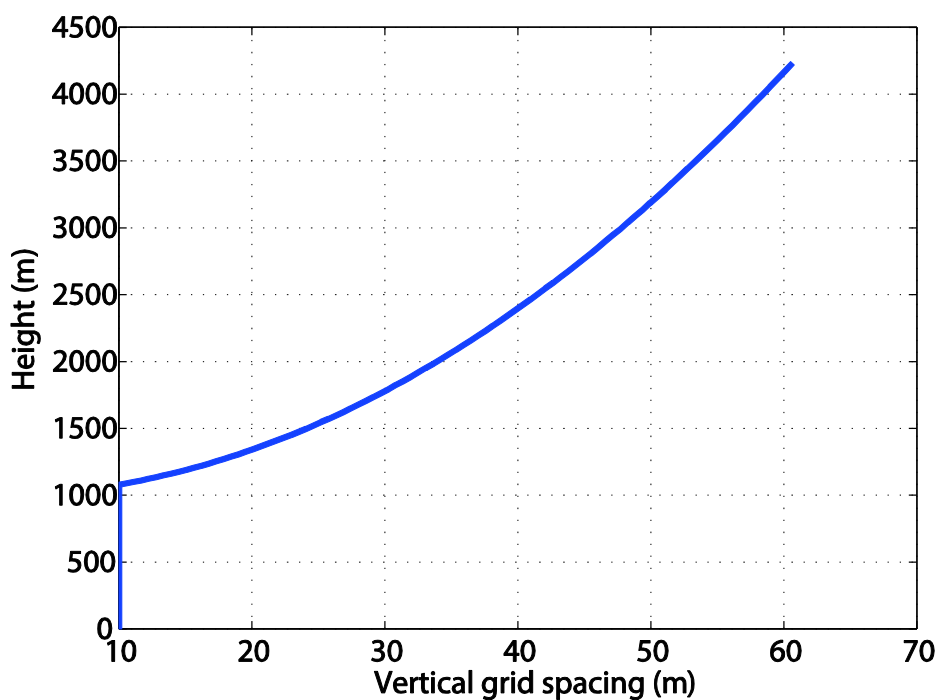
Appendix E   Simple radiation scheme

In our study we use simplified radiation scheme following (Stevens 2001),

The cooling and heating by radiation flux divergence is calculated by allowing heat to

be radiated from the saturated regions:

$$\Delta F_R = F_0 - F_0 e^{-0.85*LWP(Z,\infty)} - F_1 e^{-0.85*LWP(0,Z)}$$

$$F_0 = 70 \, W/m^2 \, in \, DYCOMS - II, \, 55 \, W/m^2 \, in \, VOCALS.$$

$$F_1 = 20 \, W/m^2 \, in \, DYCOMS - II, 15 \, W/m^2 \, in \, VOCALS.$$

In here F_0 and F_1 are derived from VVM simulation using RRTMG radiation scheme

with DYCOMS-II and VOCALS initial conditions, which represents the inversion jump

and cloud base jump value. Although such simple scheme is clearly unrealistic, it is ef-

ficient and well represents the first order effect wherein clouds efficiently concentrate

the radiative cooling of the PBL in a thin layer near cloud top and the heating near the

cloud base. Furthermore, it ensures consistency between VVM and MLM models and

significantly reduces the computational cost for this study.

Appendix F   Variables deriviation

In here we list out the variables derived from VVM output wind field, thermo, and dynamical field and water variables.

i.   *Inversion height*

Directly calculated from cloud mixing ratio q_c, at decoupling stage the lower layer is removed for derived inversion height.

ii.   *Pseudo-albedo*

Following (Zhang et al. 2005), the cloud optical depth derived from Liquid Water-Path and cloud number concentration (N_c), which is:

$$\tau = 0.19(LWP)^{5/6} \times N_c^{1/3}$$

and further, the albedo is derived from cloud optical depth:

$$A = \frac{\tau}{\tau + 6.8} + 0.1$$

in here we use $N_c = 60^{\#}cm^{-3}$ stands for non-precipitating stratocumulus and 0.1 represents the sea surface albedo.

iii.   *Buoyancy Integral Ratio (BIR)*

$$BIR \equiv -\frac{\int_0^{zi} \overline{w'b'} \ dz, \ in \ which \ \overline{w'b'} < 0}{\int_0^{zi} \overline{w'b'} \ dz, \ in \ which \ \overline{w'b'} > 0}$$

iv.   *Total water mixing ratio Difference ($q_t d$)*

$$q_t d \equiv q_t(0.25zi) - q_t(0.75zi)$$

v.   *Velocity scale w_c*

$$[2.5\beta g \int_0^{zi} \overline{w's'_v} dz\,]^{1/3}$$

vi.   *Normalized vertical Integrated Turbulent Kinetic Energy (normalized ITKE)*

$$\frac{1}{2}(\overline{u'^2} + \overline{v'^2} + \overline{w'^2}) \Big/ (w_c^2 z_i)$$

vii.   *Turbulent mass flux*

$$M = \sum_i \sigma_i \times (w_i - \overline{w})$$

Where, σ_i is the fraction of i_{th} vertical velocities at certain level, w_i is the i_{th}

vertical velocity bins and $\overline{w}$ is the domain average of vertical velocity.